studies and electric cortical stimulation. Electric cortical stimulation was performed using 50 Hz, bipolar, alternating square pulse of 0.3 ms duration.

3. Results

3.1. Delineation of epileptogenic area

She had five CPSs during the invasive monitoring period, and none of them were preceded by her typical aura. Subdural EEG showed that three seizures started with low-voltage fast activities in the posterior part of the right mesial temporal area (bold circles, Fig. 2A) followed by burst of spikes, and then spread to the lateral part. Clinical manifestation of one of them consisted of motion arrest followed by oral and bilateral hand automatisms, and the other two showed motion arrest only. One seizure with motion arrest started with low-voltage fast activities at one electrode (C4, shaded circle in Fig. 2A) in the anterior lateral temporal area, spread to basal temporal area showing rhythmic spikes. The other seizure with motion arrest and oral and bilateral hand automatisms started with spikes in the posterior part of the right lateral electrodes (A6 and A11, oblique lines in Fig. 2A). Additionally she had two habitual auras during invasive monitoring, but no EEG changes occurred. Interictal spikes were frequently seen in the mesial side of the posterior basal temporal area, and quickly spread to the adjacent electrodes (Fig. 2B and C).

3.2. Functional mapping

Pattern-reversal, visual stimulation of the fovea (3° × 3°) and central visual field (10° × 10°) evoked responses in the basal temporal area adjacent to the most active epileptogenic focus (Fig. 3). Left peripheral hemifield stimulation elicited evoked potentials in the more mesial area, while no responses were seen to the right peripheral hemifield stimulation. Median and tibial SEP and AEP showed non-primary responses at the electrodes located on the lateral superior temporal areas. Electric cortical stimulation at the basal temporal electrodes in the vicinity of the area where VEP was evoked elicited elementary and complex hallucinations in the left upper visual field in the absence of afterdischarges or her habitual auras (Fig. 4).

3.3. Surgical outcome and seizure control

The most active epileptic region in the right mesial basal temporal area within the MCD was resected tailored by

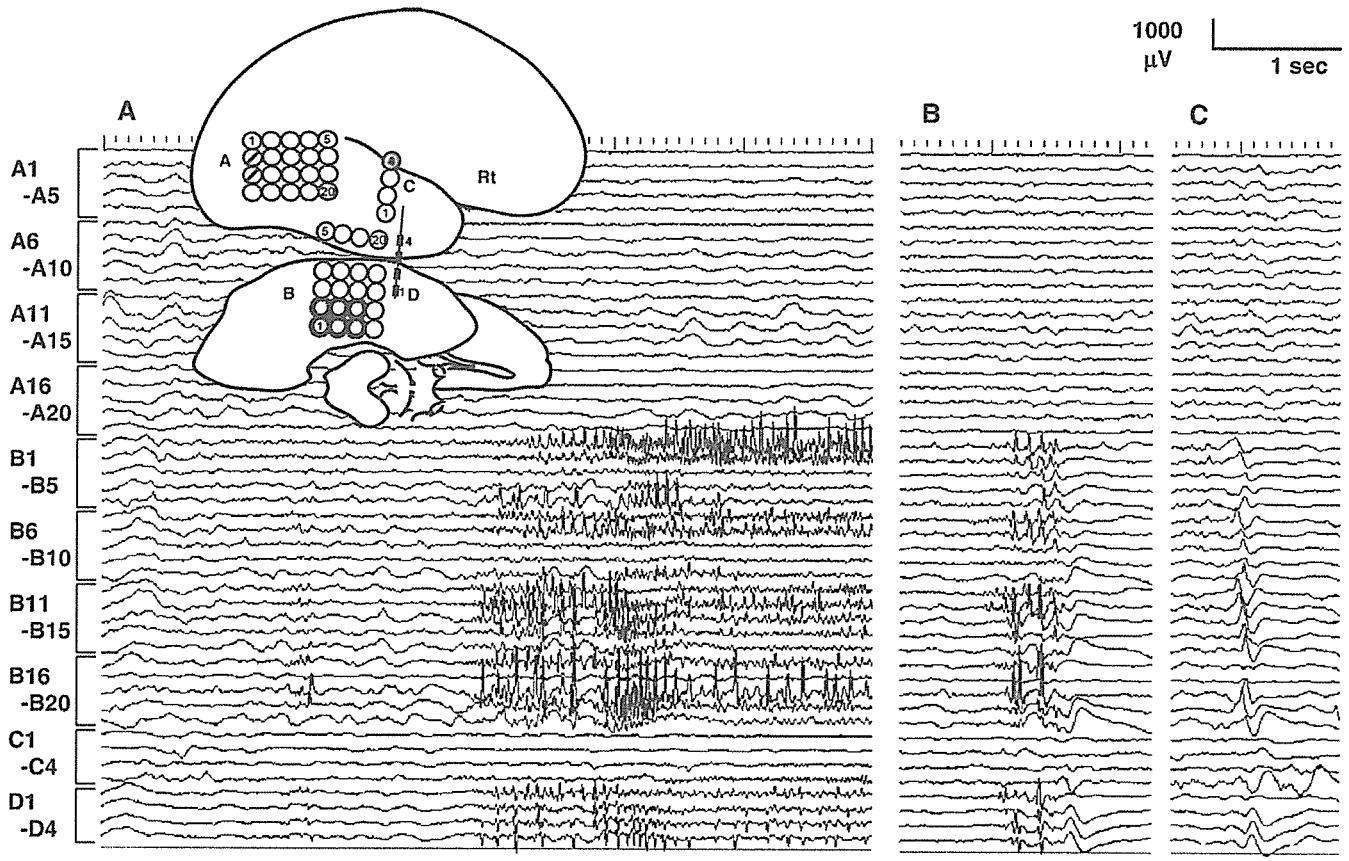

Fig. 2. Invasive EEG records. (A) Recording of a habitual seizure. Electrographic seizures most frequently started from the posterior part of the right mesial temporal area (bold circles, subdural record) approximately 15 s before the clinical onset; these areas were resected. A shaded circle and circles with oblique lines indicate other epileptogenic foci with lesser activity. (B, C) Interictal record. Interictal spikes were frequently seen in the mesial side of the posterior basal temporal area, and easily spread to the adjacent electrodes.

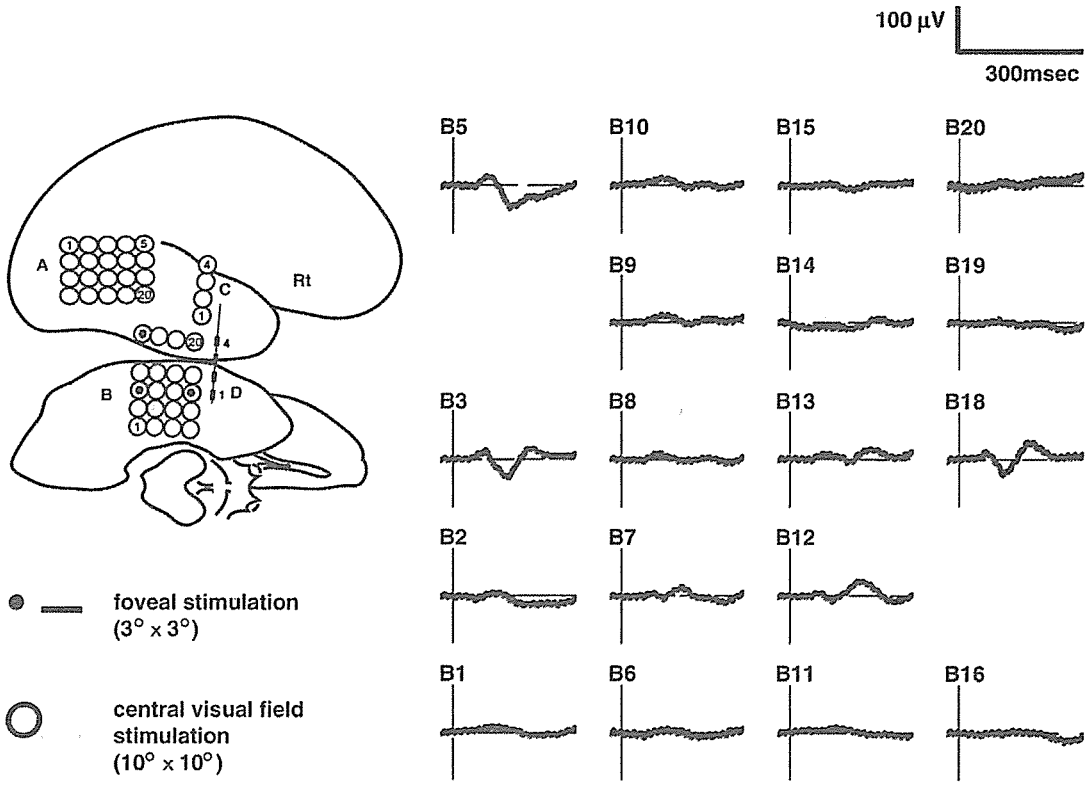

Fig. 3. VEP recording in the right basal temporal area (B plate). Foveal (dots, thick lines) and central visual field stimulation (shaded circles, gray lines) elicited responses adjacent to the most active epileptogenic area. Epilepsy surgery was performed with the best effort to spare the functional area as much as possible.

invasive EEG using subdural and depth electrodes (Figs. 1G–I and 2A) with the best effort to spare the functional area as much as possible. Histological diagnosis of the resected epileptogenic area of the patient was type IA cortical dysplasia without any balloon cells (BCs). The patient developed no neurological deficits after resection. During

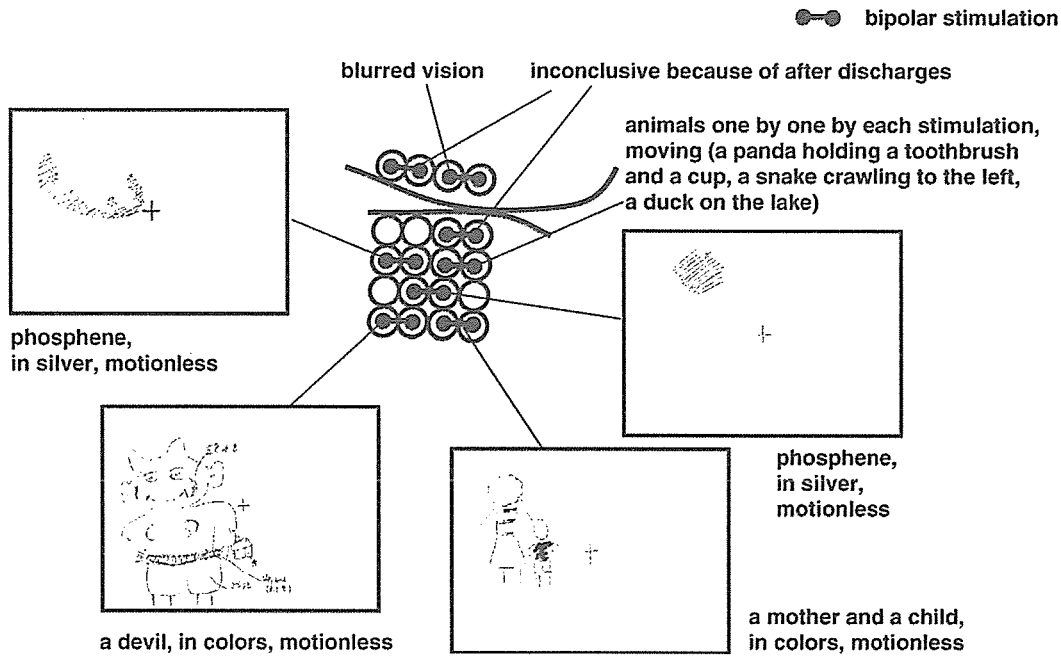

Fig. 4. Electric cortical stimulation at the basal temporal electrodes in the vicinity of the area where VEP was evoked (B plate, see Fig. 3). Elementary and complex hallucinations were elicited in the left upper visual field. Reproducibility of the symptoms was confirmed in the absence of afterdischarges or auras (insets are patient's own drawings of what she saw during stimulation).

two months after surgery the patient developed non-epileptic auditory hallucination consisting of the feeling that somebody was always talking to and chasing her, and they were totally different from her habitual auras. Before surgery, the patient had experienced the similar symptom only twice. This psychotic event was successfully controlled by neuroleptic medication of risperidone and olanzapine, therefore we consider it as post operative psychosis associated with forced normalization [11]. After a follow-up period of 2 years, the patient was in Engel's class IIA.

4. Discussion

This case demonstrated the presence of heterogeneous epileptogenicity within MCD by means of invasive EEG recording. Invasive EEG findings during habitual seizures and of interictal period suggested multiple foci within the lesion, and the most active epileptogenic region was found in the mesial side of the right basal temporal area, whose histopathology showed a mild cortical dysplasia without any BCs. The present finding is in accordance with a previous report which demonstrated, within individual MCD, that dysplastic lesions containing BCs (type IIB) were less epileptogenic than those without BCs (type I and type IIA) [2].

VEP in the present patient demonstrated that the MCD lesion in the basal temporal area participated in visual processing. In this patient, high-amplitude cortical potentials were elicited by central, foveal and left peripheral hemifield stimulation but not by right peripheral hemifield stimulation, suggesting that this cortical area possessed the function of the primary visual cortex. However, the broad distribution of VEP with the most prominent potentials in the mesial part of basal temporal area differed from the well-known, strict localization of high-amplitude responses [12]. This difference is possibly explained by atypical organization of cortical function in the present patient, as shown in previous PET and functional MRI studies [6,7]. Moreover, this patient showed elementary and complex visual hallucinations when the basal temporal area was stimulated. Elementary hallucinations occur with the involvement of the primary visual cortex [13], and thus if they were observed during spontaneous temporal lobe seizures or upon electrical stimulation of the temporal lobe, usually they were explained by the spread of activity to the occipital lobe [13]. Therefore, elementary hallucinations in this patient produced by electric stimulation suggest the atypical location of the primary visual cortex in the basal temporal area.

In summary, this case report demonstrated that the seizure reduction with sparing the functional area can be achieved by precise presurgical evaluation using subdural electrodes, including electric cortical stimulation, recordings of habitual seizures and evoked potentials. More case accumulation is warranted to prove the notion that it is possible to achieve not only the maximum seizure reduction but also the minimum functional deficits by epilepsy surgery.

Acknowledgment

The authors thank Dr. Akira Sengoku, Sengoku clinic, Kyoto-shi, Japan, for referring the patient. This study was supported by the Research Grant for the Treatment of Intractable Epilepsy (16-1) from the Japan Ministry of Health, Labour and Welfare, and Scientific Research Grant (C2) from the Japan Society for Promotion of Science (JSPS).

References

[1] Kuzniecky RI, Jackson GD. Developmental disorders. In: Engel Jr J, Pedley TA, editors. Epilepsy A Comprehensive Textbook. Philadelphia: Lippincott-Raven; 1997, p. 2517–32.
[2] Boonyapisit K, Najm I, Klem G, Ying Z, Burrier C, LaPresto E, et al. Epileptogenicity of focal cortical malformations due to abnormal cortical development: direct electrocorticographic–histopathologic correlations. Epilepsia 2003;44(1):69–76.
[3] Francione S, Vigliano P, Tassi L, Cardinale F, Mai R, Lo Russo G, et al. Surgery for drug resistant partial epilepsy in children with focal cortical dysplasia: anatomical–clinical correlations and neurophysiological data in 10 patients. J Neurol Neurosurg Psychiatry 2003;74:1493–501.
[4] Chassoux F, Devaux B, Landré E, Turak B, Nataf F, Varlet P, et al. Stereoelectroencephalography in focal cortical dysplasia. A 3D approach to delineating the dysplastic cortex. Brain 2000;123:1733–51.
[5] Palmini A, Gambardella A, Andermann F, Dubeau F, da Costa JC, Olivier A, et al. Operative strategies for patients with cortical dysplastic lesions and intractable epilepsy. Epilepsia 1994;35:S57–71.
[6] Janszky J, Ebner A, Kruse B, Mertens M, Jokeit H, Seitz RJ, et al. Functional organization of the brain with malformations of cortical development. Ann Neurol 2003;53:759–67.
[7] Richardson MP, Koepp MJ, Brooks DJ, Coull JT, Grasby P, Fish DR, et al. Cerebral activation in malformations of cortical development. Brain 1998;121:1295–304.
[8] Innocenti GM, Maeder P, Knyazeva MG, Fornari E, Deonna T. Functional activation of microgyric visual cortex in a human. Ann Neurol 2001;50:672–6.
[9] Mikuni N, Ikeda A, Yoneko H, Amano S, Hanakawa T, Fukuyama H, et al. Surgical resection of an epileptogenic cortical dysplasia in the deep foot sensorimotor area. Epilepsy Behav 2005;7:559–62.
[10] Takayama M, Miyamoto S, Ikeda A, Mikuni N, Takahashi JB, Usui K, et al. Intracarotid propofol test for speech and memory dominance in man. Neurology 2004;63:510–5.
[11] Andermann LF, Savard G, Meencke HJ, McLachlan R, Moshe S, Andermann F. Psychosis after resection of ganglioglioma or DNET: evidence for an association. Epilepsia 1999;40:83–7.
[12] Noachtar S, Hashimoto T, Lüders H. Pattern visual evoked potentials recorded from human occipital cortex with chronic subdual electrodes. Electroencephalogr Clin Neurophysiol 1993;88:435–46.
[13] Bien CG, Benninger FO, Urbach H, Schramm J, Kurthen M, Elger CE. Localizing value of epileptic visual auras. Brain 2000;123:244–53.

Journal of Neuroscience Research 85:153–165 (2007)

Presenilin 1 Is Involved in the Maturation of β-Site Amyloid Precursor Protein-Cleaving Enzyme 1 (BACE1)

Akira Kuzuya,[1] Kengo Uemura,[1] Naoyuki Kitagawa,[1] Nobuhisa Aoyagi,[1] Takeshi Kihara,[2] Haruaki Ninomiya,[3] Shoichi Ishiura,[4] Ryosuke Takahashi,[1] and Shun Shimohama[1]*

[1]Department of Neurology, Graduate School of Medicine, Kyoto University, Kyoto, Japan
[2]Department of Neuroscience for Drug Discovery, Graduate School of Pharmaceutical Sciences, Kyoto University, Kyoto, Japan
[3]Department of Neurobiology, Tottori University, Faculty of Medicine, Yonago, Japan
[4]Department of Life Sciences, Graduate School of Arts and Sciences, University of Tokyo, Tokyo, Japan

One of the pathologic hallmarks of Alzheimer's disease is the excessive deposition of β-amyloid peptides (Aβ) in senile plaques. Aβ is generated when β-amyloid precursor protein (APP) is cleaved sequentially by β-secretase, identified as β-site APP-cleaving enzyme 1 (BACE1), and γ-secretase, a putative enzymatic complex containing presenilin 1 (PS1). However, functional interaction between PS1 and BACE1 has never been known. In addition to this classical role in the generation of Aβ peptides, it has also been proposed that PS1 affects the intracellular trafficking and maturation of selected membrane proteins. We show that the levels of exogenous and endogenous mature BACE1 expressed in presenilin-deficient mouse embryonic fibroblasts (PS−/−MEFs) were reduced significantly compared to those in wild-type MEFs. Moreover, the levels of mature BACE1 were increased in human neuroblastoma cell line, SH-SY5Y, stably expressing wild-type PS1, compared to native cells. Conversely, the maturation of BACE1 was compromised under the stable expression of dominant-negative mutant PS1 overexpression. Immunoprecipitation assay showed that PS1 preferably interacts with proBACE1 rather than mature BACE1, indicating that PS1 can be directly involved in the maturation process of BACE1. Further, endogenous PS1 was immunoprecipitated with endogenous BACE1 in SH-SY5Y cells and mouse brain tissue. We conclude that PS1 is directly involved in the maturation of BACE1, thus possibly functioning as a regulator of both β- and γ-secretase in Aβ generation.

Key words: Alzheimer's disease; amyloid; γ-secretase; β-secretase

Alzheimer's disease (AD) is pathologically characterized by the excessive accumulation and deposition of β-amyloid peptides (Aβ) (Kang et al., 1987). Because the longer Aβ peptide species, Aβ1-42 (Aβ42), aggregates more readily than the shorter and more predominant species, Aβ1-40 (Aβ40), it is believed that Aβ42 plays an important role in AD pathogenesis (Hardy, 1997a,b). Aβ peptides are generated by the consecutive proteolysis of β-amyloid precursor protein (APP), by distinct enzymatic moieties known as β-secretase and γ-secretase (Golde et al., 1993; Haass et al., 1993). Recently, primary β-secretase in the brain was identified as a membrane-associated aspartyl protease, β-site APP-cleaving enzyme 1 (BACE1) (Hussain et al., 1999; Sinha et al., 1999; Vassar et al., 1999; Yan et al., 1999; Haniu et al., 2000). BACE1 generates a membrane-bound APP C-terminal fragment (APP CTFβ), which undergoes intra-membranous γ-secretase cleavage to generate the Aβ peptide. Although multiple lines of biochemical and genetic evidence have shown that γ-secretase forms high molecular weight complexes containing at least presenilin 1 (PS1), nicastrin, aph-1, and pen-2 (Capell et al., 1998; Yu et al., 2000; Edbauer et al., 2002; Francis et al., 2002; Lee et al., 2002; Steiner et al., 2002; Gu et al., 2003), the functional interaction of β- and γ-secretase in Aβ generation still remains unclear.

Importantly, mutations in PS1 are the most common known cause of autosomal dominant familial Alzheimer's disease (FAD) (Rogaev et al., 1995; Sherrington et al., 1995; Thinakaran 1999). These mutations increase the level of Aβ42/40 in transfected mammalian cells and the

Contract grant sponsor: Ministry of Education, Culture, Sports, Science and Technology of Japan; Contract grant sponsor: Japan Society for the Promotion of Science; Contract grant sponsor: Ministry of Health, Labour and Welfare of Japan; Contract grant sponsor: Smoking Research Foundation; Contract grant sponsor: Philip Morris USA, Inc.; Contract grant sponsor: Philip Morris International.

*Correspondence to: Dr. Shimohama, Department of Neurology, Graduate School of Medicine, Kyoto University, 54 Shogoin-Kawaharacho, Sakyo-ku, Kyoto 606-8507, Japan.
E-mail: i53367@sakura.kudpc.kyoto-u.ac.jp

Received 20 January 2006; Revised 25 May 2006; Accepted 4 September 2006

Published online 30 October 2006 in Wiley InterScience (www.interscience.wiley.com). DOI: 10.1002/jnr.21104

brains of transgenic mice (Borchelt et al., 1996; Duff et al., 1996). Whereas it has generally been accepted that PS1 is the essential catalytic component of γ-secretase (Wolfe et al., 1999a,b), it has also been reported that Aβ is still generated in absence of both PS1 and its homologue PS2 (Armogida et al., 2001; Wilson et al., 2002). In addition, it has also been proposed that PS1 affects the intracellular trafficking and maturation of selected membrane proteins. Indeed, PS1 deficiency affects the intracellular trafficking and maturation of TrkB, as well as ICAM5/telenchephalin in neurons (Naruse et al., 1998; Annaert et al., 2001). We have also shown that PS1 regulates the intracellular trafficking and maturation of N-cadherin in SH-SY5Y cells (Uemura et al., 2003a). Furthermore, it has been shown that PS1 is involved in regulating the intracellular trafficking and maturation of APP and nicastrin, which are essential for Aβ generation (Kim et al., 2001; Edbauer et al., 2002; Leem et al., 2002a,b; Cai et al., 2003; Herreman et al., 2003). Although there is no reported genetic linkage between mutations in BACE1 and AD to date, recent reports have shown an elevation of BACE1 protein expression and its enzymatic activity in AD brains (Fukumoto et al., 2002; Holsinger et al., 2002; Yang et al., 2003), indicating that BACE1, as well as PS1, is involved significantly in AD pathogenesis. Recently, Kamal et al. (2001) showed that APP, PS1, and BACE1 are transported in the same membrane vesicles along the axons in vivo, via the direct binding of APP to the kinesin light chain subunit of kinesin-I, a microtubule motor protein. These observations raise the possibility that PS1 is related functionally to the intracellular trafficking and maturation of BACE1 through the amyloidogenic pathway of APP.

Based on the above observations, we hypothesized that PS1 influences the intracellular trafficking and maturation of BACE1. To characterize the effect of PS1 on the trafficking-dependent maturation of BACE1, wild-type (wt) and presenilin-deficient mouse embryonic fibroblast cell lines (MEFs) or human neuroblastoma SH-SY5Y cell lines stably expressing either wt PS1 or dominant-negative PS1 were used in the present study. We report that wt PS1 binds BACE1 directly and upregulates its maturation, whereas the absence of PS1 or dominant-negative PS1 downregulates its maturation. Taking the previous reports and our results together, we suggest that PS1 significantly modulates both β- and γ-secretase via regulation of the intracellular trafficking of both secretase, and operates as a primary regulator determining the amyloidogenic processing of APP.

MATERIALS AND METHODS

Cell Cultures, Constructs, Transfection and Brain Tissue

The generation of SH-SY5Y cells stably expressing either wild-type PS1 (wt PS1) or dominant-negative (D385A) PS1 has been described previously (Uemura et al., 2003b). In the present experiments, we used native SH-SY5Y cells as control cells. Wild-type (wt) and PS1/PS2 (PS−/−) double knockout mouse embryonic fibroblast (MEF) cell lines (Herreman et al., 1999, 2003) were kindly provided by Dr. De Strooper (Center for Human Genetics, KUL, VIB, Belgium). These cell lines were maintained in Dulbecco's modified Eagle's medium (DMEM; Nissui Pharmaceutical, Tokyo, Japan) containing 10% fetal bovine serum (FBS), 100 IU/ml penicillin, 100 μg/ml streptomycin and glutamine (2 mM) (Life Technologies, Rockville, MD) at 37°C in 5% CO_2. Stably transfected SH-SY5Y cells were selected and maintained with 300 mg/ml G418 (Wako Pure Chemical Industries, Ltd., Osaka, Japan). For immunoprecipitation experiment using the SH-SY5Y cell lines, the cells were cultured in Opti-MEM I (Gibco BRL, Rockville, MD) containing 10% FBS to grow at full confluency. An expression vector to encode HA-tagged human full-length BACE1 has been described previously (Hattori et al., 2002). An expression vector to encode FAD-linked PS1 mutant containing proline (Pro) to leucine mutation at position Pro-117 (P117L PS1) has been described previously (Uemura et al., 2003b). An expression vector to encode GFP was purchased from Invitrogen. Lipofectamine 2000 (Invitrogen Life Technologies) was used for transient cotransfection of BACE1 and GFP constructs into MEF cells, according to the instruction. During and after the transfection, cells were maintained in Opti-MEM I. GFP was cotransfected with BACE1, using as an indicator of transfection efficiency. To obtain comparable expression levels of GFP between wt and PS−/− MEF cells, the transfection condition was optimized by varying doses of DNA and Lipofectamine 2000. Rat primary cultures were obtained from the fetal rat cerebral cortex (17–19 days gestation) and were maintained as described previously (Kihara et al., 1997). Mouse primary cultures were prepared as described previously (Uemura et al., 2006). Only mature neurons were used for the present experiments. For the treatment of γ-secretase inhibitors to primary cultures, the medium containing either 2 μM L-685,458 or 1 μM DAPT were exchanged every day for 4 days. Control cells were treated with vehicle (DMSO) only. Fresh brain tissue was prepared from 3-month-old mice. The animals were treated in accordance with the guidelines published in the National Institutes of Health Guide for the Care and Use of Laboratory Animals.

Antibodies and Reagents

Monoclonal antibody MAB5308 against the C terminus of BACE1, monoclonal antibody MAB5232 against the loop domain of PS1 and rabbit polyclonal anti-mannosidase II antibody were purchased from Chemicon (Temecula, CA). Monoclonal and rabbit polyclonal anti-HA antibodies, monoclonal anti-β-actin antibody, rabbit polyclonal anti-APP antibody recognizing the C terminus and rabbit polyclonal anti-BACE1 antibody, EE-17, recognizing the N terminus (amino acids 46–62), were purchased from Sigma (St. Louis, MO). Rabbit polyclonal anti-proBACE1 antibody (targeting amino acids 26–45 corresponding to the prodomain sequence), rabbit polyclonal anti-BACE1 antibody (targeting amino acids 485–501) and rabbit polyclonal anti-BACE1 antibody (targeting amino acids 487–501) were purchased from Calbiochem. Rabbit polyclonal anti-calnexin antibody was purchased from StressGen (Victoria, BC). Rabbit polyclonal anti-PS1 antibody against the N terminus was purchased from Santa Cruz Biotechnology (Santa Cruz, CA). Rabbit polyclonal anti-GFP antibody was purchased from

TABLE I. Antibodies used in Experiment

Antigen	Name	Epitope	Host
BACE1	MAB5308	C-terminus	Monoclonal
	Anti-BACE1	C-terminus (aa 487–501)	Polyclonal rabbit
	Anti-BACE1	C-terminus (aa 485–501)	Polyclonal rabbit
	EE-17	N-terminus (aa 46–62)	Polyclonal rabbit
	Anti-proBACE1	Prodomain (aa 26–45)	Polyclonal rabbit
PS1	Anti-PS1	N-terminus	Polyclonal rabbit
	MAB5232	Loop domain	Monoclonal

Molecular Probes (Eugene, OR). For immunostaining, Alexa Fluor 546 goat anti-mouse IgG (H+L) conjugate and Alexa Fluor 488 goat anti-rabbit IgG (H+L) conjugate (Molecular Probes) were used as secondary antibodies. In Table I, the corresponding epitopes of anti-PS1 and anti-BACE1 antibodies used in the present experiment are summarized. Two well-characterized γ-secretase inhibitors, L-685,458 and *N*-[*N*-(3,5-difluorophenacetyl)-L-alanyl]-*S*-phenylglycine *t*-butyl ester (DAPT) were purchased from Sigma and Calbiochem, respectively.

Reverse Transcription-Polymerase Chain Reaction

Total RNA was extracted from confluent cells of each cell line by using ISOGEN (Nippon Gene, Toyama, Japan). Equal amounts of total RNA obtained from each cell line were processed for cDNA synthesis using oligo (dT) primers and reverse transcriptase, using a RNA LA PCR kit (AMV) (TaKaRa, Tokyo, Japan). They were amplified by polymerase chain reaction (PCR) using sense and anti-sense primers specific for either the human *BACE1* gene (5′CATTGGAGGTATCGACCACTCGCT3′ and 5′CCACAGTCTTCCATGTCCAA-GGTG3′, the product size was 624 bp; GenBank accession number AF190725) or the human *glyceraldehyde-3-phosphate dehydrogenase* (*GAPDH*) gene (5′ACCACAGTCCATGCCATCAC3′ and 5′TCCACCACCCTGTTGCTGTA3′, 452 bp; J04038). The amplification program consisted of a denaturing step at 94°C for 1 min, an annealing step at 62°C for 40 src, and an extension step at 72.9°C for 50 sec. This was repeated 25 cycles for BACE and 18 cycles for GAPDH. The PCR products separated on a 1.5% agarose gel were stained by ethidium bromide and visualized using a UV transilluminator coupled to a CCD camera.

Preparation of Protein Samples, Western Blot Analysis, and immunoprecipitation

Confluent cells were rinsed three times with ice-cold phosphate-buffered saline (PBS) and centrifuged. Each pellet was suspended in TNE buffer (10 mM Tris-Hcl, pH 7.8, 1% NP40, 0.15 M NaCl, 1 mM EDTA) supplemented with 1 mM dithiothreitol (DTT) and 1 mM phenylmethylsulphonyl fluoride (PMSF), dispersed by pipetting vigorously 20 times and then rotated for 1 hr at 4°C. Each sample was then centrifuged at 25,000 × *g* for 30 min at 4°C and the supernatants were collected to obtain the protein samples. Protein concentration was determined using the Bradford assay (Bradford, 1976). Equal amounts of protein were treated with Protein G-Sepharose (Amersham Biosciences, Uppsala, Sweden) overnight at 4°C. After removing Protein G-Sepharose by centrifugation at 2,000 × *g* for 5 min, either the MAB5308 antibody, the anti-BACE1 antibody (Calbiochem), or anti-PS1 antibody (Santa Cruz Biotechnology, Santa Cruz, CA) was added to the lysate. Each sample was rotated for 1 hr at 4°C and then treated with Protein G-Sepharose for 1 hr at 4°C. The immunoprecipitates were washed with TNE buffer five times and resuspended in 2× sample buffer (125 mM Tris-HCl [pH 6.8], 4.3% SDS, 30% glycerol, 10% 2-mercaptoethanol, and 0.01% bromophenol blue). After boiling for 3 min, the supernatants were subjected to Western blotting. For the detection of full-length PS1, the suspension was incubated at 37°C for 10 min instead of boiling. Alternatively, confluent cells were rinsed three times with ice-cold PBS and scraped off. Cell pellets were suspended in TNE buffer supplemented with 1 mM DTT and 1 mM PMSF, and sonicated. The samples were centrifuged at 25,000 × *g* for 30 min at 4°C and the supernatants were collected to obtain protein samples. Protein concentration was determined using the Bradford assay, and then equal amounts of cell extracts were subjected to Western blotting.

In Western blot analysis, samples were electrophoresed on polyacrylamide gels in the presence of SDS. Immunoblotting was carried out by transferring the proteins to polyvinylidene difluoride microporous membrane, which was then blocked with 5% skimmed milk in 10 mM PBS containing 0.1% Tween 20 (PBS-T), and incubated with the primary antibodies in PBS-T containing 4% BSA overnight at 4°C. The membranes were then washed in PBS-T and incubated with a horseradish peroxidase-conjugated anti-mouse or anti-rabbit IgG (Amersham, Little Chalfont, UK) in PBS-T for 1 hr at room temperature. The specific reaction was visualized, using the enhanced chemiluminescence method (ECL) (Amersham).

Immunostaining

Immunostaining was carried out as described previously (Uemura et al., 2003b). Briefly, SH-SY5Y cell lines and 5 days in vitro primary cultures were fixed with 4% paraformaldehyde for 20 min. Fixed cells were blocked with 3% BSA in PBS with 0.2% Triton X-100 for 15–20 min and incubated overnight at 4°C with primary antibodies diluted in PBS containing 3% BSA. Immunoreactivity was visualized using the species-specific secondary antibodies mentioned above. Samples were observed using a LSM (Zeiss) confocal scanning microscope.

Statistical Analysis

The relative density of the bands in RT-PCR or Western blot was analyzed by quantitative densitometry using a computerized image analysis program (NIH Image 1.59). To compare either the levels of mature BACE1 or the mature:proBACE1 ratio among the SH-SY5Y cell lines, statistical analysis was carried out using one-way ANOVA, followed by post-hoc Fisher's protected least significant difference. To compare the mature BACE1:GFP ratio or the mature:proBACE1 ratio between wt MEFs and PS−/− MEFs, statistical analysis was carried out using Student's *t*-test. Data were expressed as the mean ± SD, and significance was assessed at $P < 0.01$.

RESULTS

PS1 Is Involved in BACE1 Maturation

Previous studies showed that BACE1 undergoes core glycosylation in the endoplasmic reticulum (ER) cotranslationally, and is produced as proBACE1. Then, short-lived proBACE1 is transported from the ER to the Golgi apparatus, and undergoes rapid maturation by the proteolytic removal of the prodomain followed by complex *N*-glycosylation in the Golgi apparatus (Capell et al., 2000; Haniu et al., 2000; Huse et al., 2000; Creemers et al., 2001). Finally, mature BACE1 is quite stable unlike proBACE1, and is located in the late secretory compartments, the plasma membrane, and the endosomal compartments (Huse et al., 2000; Walter et al., 2001).

To examine a possible role for PS1 in regulating BACE1 maturation, we first investigated the effect of PS deficiency on BACE1 maturation, using PS1 and its homologue PS2 double-knockout (PS−/−) mouse embryonic fibroblasts (MEFs) (Herreman et al., 1999, 2003). HA-tagged wt BACE1 and GFP plasmids were transiently cotransfected into wt and PS−/− MEFs, and the cells were collected 24 hr after transfection. Each cell lysate was subjected to Western blot analysis using either monoclonal anti-HA antibody or anti-GFP antibody. As shown in Figure 1A, the immunoblotting bands of HA-tagged BACE1 were detected as two different molecular weight bands. The higher molecular weight bands represented mature BACE1, complex N-glycosylated one, whereas the lower molecular weight bands represented proBACE1, a precursor of mature BACE1 (Capell et al., 2000). Interestingly, the levels of mature BACE1 were apparently reduced in PS−/− MEFs compared to wt MEFs, whereas the levels of GFP were comparable between them, indicating that the transfection efficiency was not different (Fig. 1A). Quantitative analysis showed that the ratio of mature BACE1:GFP was reduced by 70% in PS−/− MEFs, compared to that in wt MEFs (Fig. 1B; n = 4, $P < 0.0005$). In addition, the ratio of mature:proBACE1 was reduced by 50% in PS−/− MEFs, compared to that in wt MEFs (Fig. 1C, n = 4, $P < 0.0005$). These data suggest that the expression level of PS affects significantly the maturation of BACE1 in MEF cells. To further confirm the effect of PS expression on BACE1 maturation at endogenously expressed level, we compared the levels of endogenous BACE1 between wt and PS−/− MEFs. Equal amounts of cell lysates obtained from wt and PS−/− MEFs were subjected to Western blotting, using anti-BACE1 antibody (targeting amino acid 485–501), and anti-proBACE1 antibody. Lysates of mouse brain tissue and mouse primary neurons were used as positive controls. As expectedly, the level of mature BACE1 in PS−/− MEFs was reduced drastically as compared to that in wt MEFs, whereas the levels of β actin were almost constant between them (Fig. 1D). Interestingly, we observed no significant difference in the levels of proBACE1 between them, indicating that the maturation of endogenous BACE1 was remarkably inhibited in PS−/− MEFs as compared to in wt MEFs (Fig. 1D). We then asked whether the maturation of exogenously expressed BACE1 is affected by co-expression of either wt PS1 or P117L PS1 mutant causing FAD. Plasmids to encode either GFP, wt PS1, or P117L PS1 were cotransfected with HA-tagged BACE1 plasmid into PS−/− MEFs by 1:1 ratio. The cells were collected 24 hr after transfection, and each cell lysate was subjected to Western blotting analysis using either rabbit polyclonal anti-HA antibody or anti-PS1 antibody (against the N terminus). As shown in Figure 1E, the levels of mature and proBACE1 were increased drastically in the cells expressing either wt PS1 or P117L PS1 as compared to those in the cells expressing GFP, whereas the levels of wt PS1 and P117L PS1 were almost similar. This result suggests that both wt PS1 and P117L PS1 similarly upregulate the stability of both mature and proBACE1 in this experimental system. The above data suggest that the expression level of PS is involved significantly in the stabilization and maturation of BACE1 in MEF cells.

To examine a specific role for PS1 in BACE1 maturation in neuronal cells, we used SH-SY5Y cells stably expressing either wild-type PS1 (wt PS1) or PS1 containing aspartate (Asp) to alanine mutation at position Asp-385 (D385A PS1). As described previously, exogenous overexpression of D385A PS1 that fails to undergo endoproteolysis, significantly replaces endogenous PS1 and results in a dominant negative version of PS1 in SH-SY5Y cells (Uemura et al., 2003b). To specifically identify either proBACE1 or mature BACE1, equal amounts of cell lysate obtained from each cell line were subjected to Western blotting using the anti-proBACE1 antibody (targeting amino acids 26–45 corresponding to the prodomain sequence) and the antibody EE-17 (targeting amino acids 46–62 corresponding to the neoepitope after removal of the prodomain), respectively. It has been reported that neoepitope antibodies specific for BACE1 after removal of the prodomain preferentially recognize the mature BACE1 polypeptide (Capell et al., 2000). Indeed, the antibody EE-17 detected the mature BACE1 polypeptide in a higher molecular weight band of 70–75 kDa that represented its complex *N*-glycosylation, whereas the anti-proBACE1 antibody detected the proBACE1 polypeptide in a tighter band of 65 kDa in lysates from each cell line (Fig. 2A). These results are consistent with the molecular weight of BACE1 described previously (Vassar et al., 1999; Capell et al., 2000; Pinnix et al., 2001). Quantitative analysis showed that the amount of mature BACE1 was increased by 20% in wt PS1 cells and was reduced by 50% in D385A PS1 cells, compared to that in control cells (Fig. 2B; n = 3, $\#P < 0.01$ vs. control, $*P < 0.0001$). Interestingly, the ratio of mature:proBACE1 was reduced significantly by 60% in D385A PS1 cells, compared to that in control cells, whereas it was not statistically different between control and wt PS1 cells (Fig. 2C; n = 3, $*P < 0.001$ vs. control).

To investigate whether the difference in BACE1 protein levels among these cell lines is dependent on the mRNA expression levels, the level of BACE1 mRNA expression in these cell lines was quantitated by semi-quantitative reverse transcription-polymerase chain reaction (RT-PCR) analysis. Expression of both BACE1 mRNA

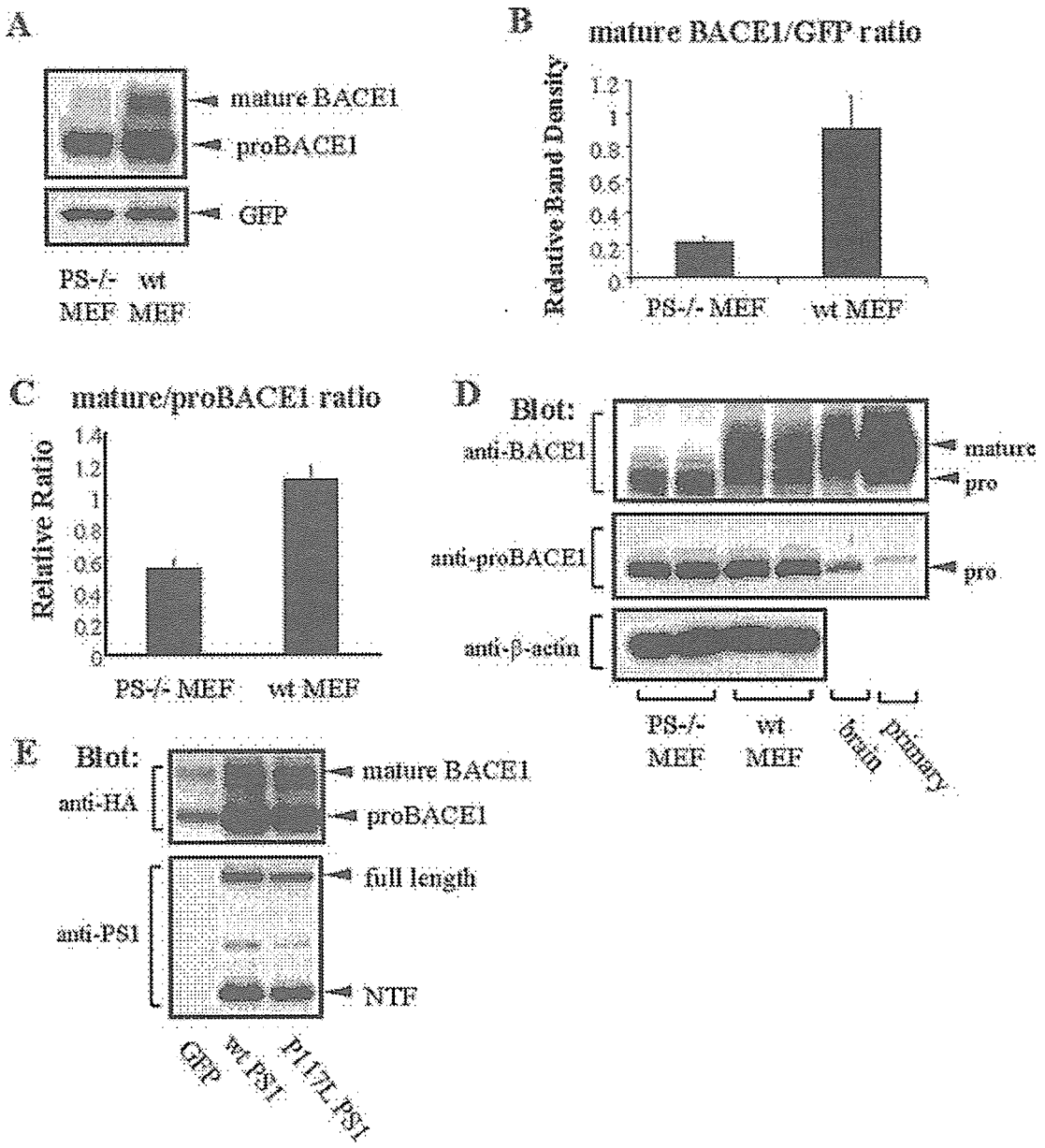

Fig. 1. PS1 is involved in BACE1 maturation post-translationally. **A:** HA-tagged BACE1 and GFP cDNA were transiently cotransfected into mouse embryonic fibroblasts (MEFs) derived from either wild-type (wt) or PS1/PS2 double-knockout (PS−/−) mice. Twenty-four hours after transfection, the cells were collected and each cell lysate was subjected to Western blot analysis and probed by either monoclonal anti-HA antibody or anti-GFP antibody. The level of mature BACE1 was apparently decreased in PS−/− MEFs as compared to that in wt MEFs, whereas the levels of GFP were almost similar between them. One representative immunoblot is shown. **B:** The band densities of either mature BACE1 or control GFP in four independent experiments were quantified by NIH imaging. The ratio of mature BACE1:GFP was calculated and analyzed by Student's *t*-test. The ratio of mature BACE1:GFP in PS−/− MEFs was significantly reduced, compared to that in wt MEFs ($n = 4$, $P < 0.0005$). **C:** The ratio of mature:proBACE1 was quantified by NIH imaging and analyzed by Student's *t*-test. The ratio of mature BACE1:proBACE1 in PS−/− MEFs was apparently reduced, compared to that in wt MEFs ($n = 4$, $P < 0.0005$). **D:** Equal amounts of cell lysates obtained from wt and PS−/− MEFs were subjected to Western blotting using the indicated antibodies. Lysates of mouse brain tissue and mouse primary neurons were used as positive controls. The endogenous level of mature BACE1 was drastically reduced in PS−/− MEFs as compared to those in wt MEFs, whereas the levels of proBACE1 were almost constant between them. One representative immunoblot is shown. **E:** Plasmids to encode either GFP, wt PS1, or P117L PS1 were cotransfected with HA-tagged BACE1 plasmid into PS−/− MEFs by 1:1 ratio. Each cell lysate was subjected to Western blotting analysis using the indicated antibodies. The levels of mature and proBACE1 were drastically increased in the cells expressing either wt PS1 or P117L PS1 as compared to those in the control cells. One representative immunoblot is shown.

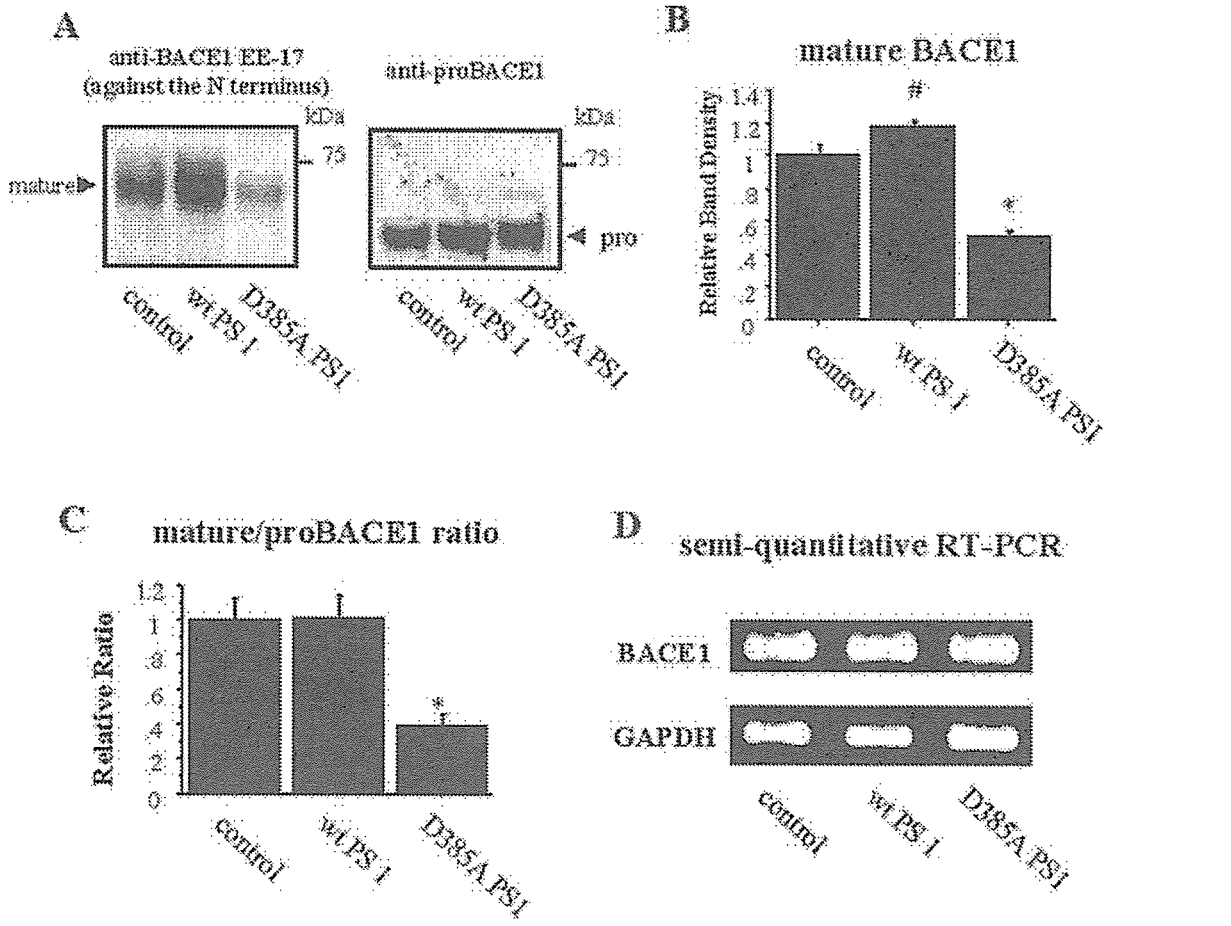

Fig. 2. **A:** Protein levels of BACE1 were compared between control SH-SY5Y cells and SH-SY5Y cells stably expressing either wt PS1 or D385A PS1. Equal amounts of whole cell lysates were subjected to Western blotting using the indicated antibodies. Mature BACE1 polypeptide was identified as a higher band of 70–75 kDa, whereas pro-BACE1 polypeptide was identified as a tighter band of 65 kDa. **B:** Immunoblotting of the mature BACE1 in each cell line was quantified by NIH imaging and analyzed by one-way ANOVA. The level of mature BACE1 was significantly reduced in D385A PS1 cells and increased in wt PS1 cells ($n = 3$, $^{\#}P < 0.01$ vs. control, $^{*}P < 0.0001$). **C:** The ratio of mature:proBACE1 in each cell line was quantified by NIH imaging and analyzed by one-way ANOVA. The ratio of mature: proBACE1 in D385A PS1 cells was significantly reduced ($n = 3$, $P < 0.001$ vs. control). **D:** The representative data of semi-quantitative RT-PCR analysis are shown. The processed cDNA was amplified by PCR using primers specific for either the human BACE1 gene or the human GAPDH gene. No significant differences in the levels of expression of BACE1 or GAPDH mRNA were observed among the cell lines.

(a 624-bp PCR product) and GAPDH mRNA (a 251-bp PCR product), a house keeping gene, were identified in these cell lines by RT-PCR analysis. The levels of BACE1 mRNA were comparable among these cell lines, whereas the levels of GAPDH mRNA were almost constant among them (Fig. 2D). Quantitative analysis, using GAPDH as an internal standard, showed that the levels of BACE1 mRNA expression were not statistically different among these cell lines (data not shown). These results indicate that the difference in BACE1 protein levels is not caused by a transcriptional regulation.

The above results suggest that wt PS1 significantly upregulates BACE1 maturation, presumably via facilitating the conversion of proBACE1 into mature BACE1 or stabilizing proBACE1. Conversely, PS deficiency and dominant–negative PS1 strongly downregulate it, indicating a novel role of PS1 for regulating BACE1 maturation.

Effect of γ-Secretase Inhibitors on BACE1 Maturation in Mouse Primary Neurons

To test whether PS1/γ-secretase activity directly affects the trafficking and maturation of BACE1 or not, we used two well-characterized γ-secretase inhibitors, L-685,458 and DAPT. Mouse primary neurons were treated with either 2 μM L-685,458, 1 μM DAPT or vehicle (DMSO) for 4 days. Equal amount of each cell lysate was subjected to Western blotting analysis using anri-BACE1 antibody (EE-17), anti-proBACE1 antibody, and anti-APP antibody (against the C terminus). As shown in Figure 3, we observed

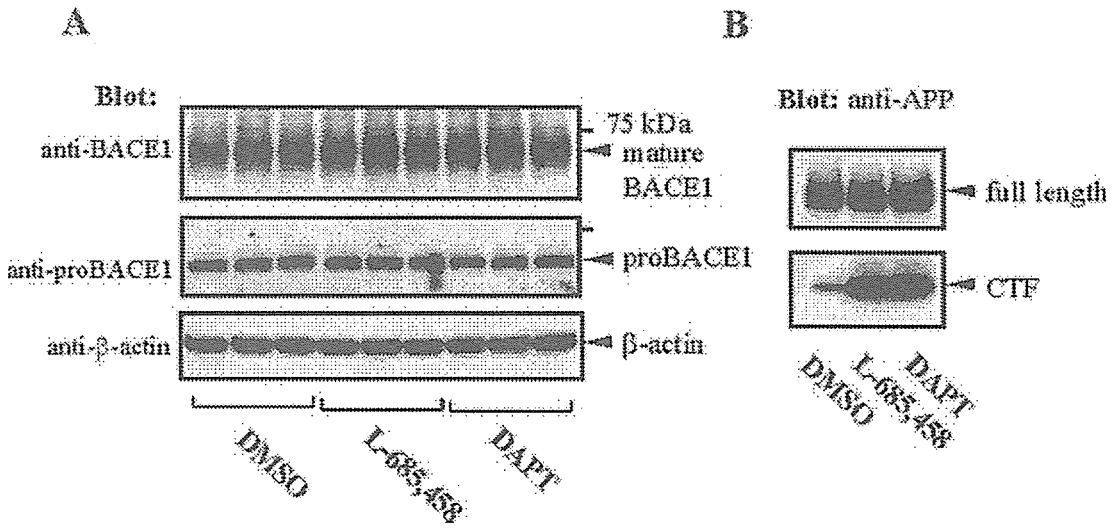

Fig. 3. Mouse primary neurons were treated with either 2 μM L-685,458, 1 μM DAPT or vehicle (DMSO) for 4 days. Equal amount of each cell lysate was subjected to Western blotting analysis using the indicated antibodies. No significant difference was seen in the levels of mature and proBACE1 between each treatment group (**A**), whereas APP CTF remarkably accumulated after each γ-secretase inhibitor, indicating that γ-secretase activity was effectively inhibited (**B**). One representative immunoblot is shown.

no significant difference in the levels of mature and pro-BACE1 between each treatment group (left panel), whereas APP C-terminal fragment remarkably accumulated after L-685,458 or DAPT treatment, indicating that γ-secretase activity was effectively inhibited (right panel). Thus, we consider that PS1/γ-secretase activity itself is less likely to be involved in the maturation process of BACE1.

PS1 and BACE1 Immunoprecipitation in the Cell and the Brain Tissue

A recent report showed that PS1 directly interacts with BACE1 in double transfected human embryonic kidney 293T cells (Hebert et al., 2003). We investigated whether wt PS1 and/or D385A PS1 can be associated with BACE1 in our experimental system. To answer this question, HA-tagged BACE1 and either wt PS1 or D385A PS1 were transiently co-expressed in PS−/− MEFs. The cells were harvested about 24 hr after transfection, and equal amounts of each cell lysate was immunoprecipitated using the anti-PS1 antibody against the N terminus, followed by the Western blot analysis using monoclonal anti-HA antibody. As shown in Figure 4A, wt (lane 1) and D385A PS1 (lane 2) were apparently associated with proBACE1 but not mature BACE1 in the transfected cells.

Next, we extended our findings obtained from the analysis of MEF cells to the SH-SY5Y cell lines. Equal amounts of cell lysate obtained from each cell line were immunoprecipitated using the anti-BACE1 antibody (targeting amino acids 487–501; Calbiochem). The cell lysates (Lys) as well as the immunoprecipitates (IP) were then subjected to Western blotting using the MAB5232 antibody (against the loop domain of PS1). As shown in Figure 4B, more PS1 C-terminal fragment (CTF) immunoreactivity was observed in wt PS1 cells (lane 7) than in control cells (lane 6), whereas almost no PS1 CTF bound to BACE1 was detected in D385A PS1 cells (lane 8; lower panel), reflecting the diminished endoproteolysis of D385A PS1 (lane 3). Conversely, solid association between the full-length D385A PS1 and BACE1 was observed (Fig. 4B, lane 8; upper panel). Furthermore, we showed the in vivo interaction between PS1 CTF and BACE1, using adult mouse brain tissue (Fig. 4C). The above results indicate that PS1 is preferably bound to proBACE1 rather than mature BACE1 and the functional binding can be contributed to the maturation of BACE1.

PS1 and BACE1 Colocalization in the SH-SY5Y Cells and Primary Neurons

To support the interaction between PS1 and BACE1 obtained from the immunoprecipitation experiment, we examined the intracellular localization of these two biochemical partners by immunofluorescent confocal microscopy, using control, wt PS1, and D385A PS1 SH-SY5Y cells. After permeabilization, cells were doubly stained with the antibody MAB5308 to visualize BACE1 and the anti-PS1 antibody (against the N terminus) to visualize PS1. As shown in Figure 5A–C, the PS1 in each cell line largely colocalized with the endogenous BACE1. Consistent with the above result shown in Figure 2A, an increase in wt PS1 immunoreactivity was apparently accompanied by an increase in endogenous BACE1 immunoreactivity (Fig. 5B, compared to 5A).

To further confirm the colocalization of PS1 and BACE1 in physiologically relevant system, endogenous PS1 and BACE1 were doubly immunostained in rat primary cultured cortical neurons at 5 days in vitro, using

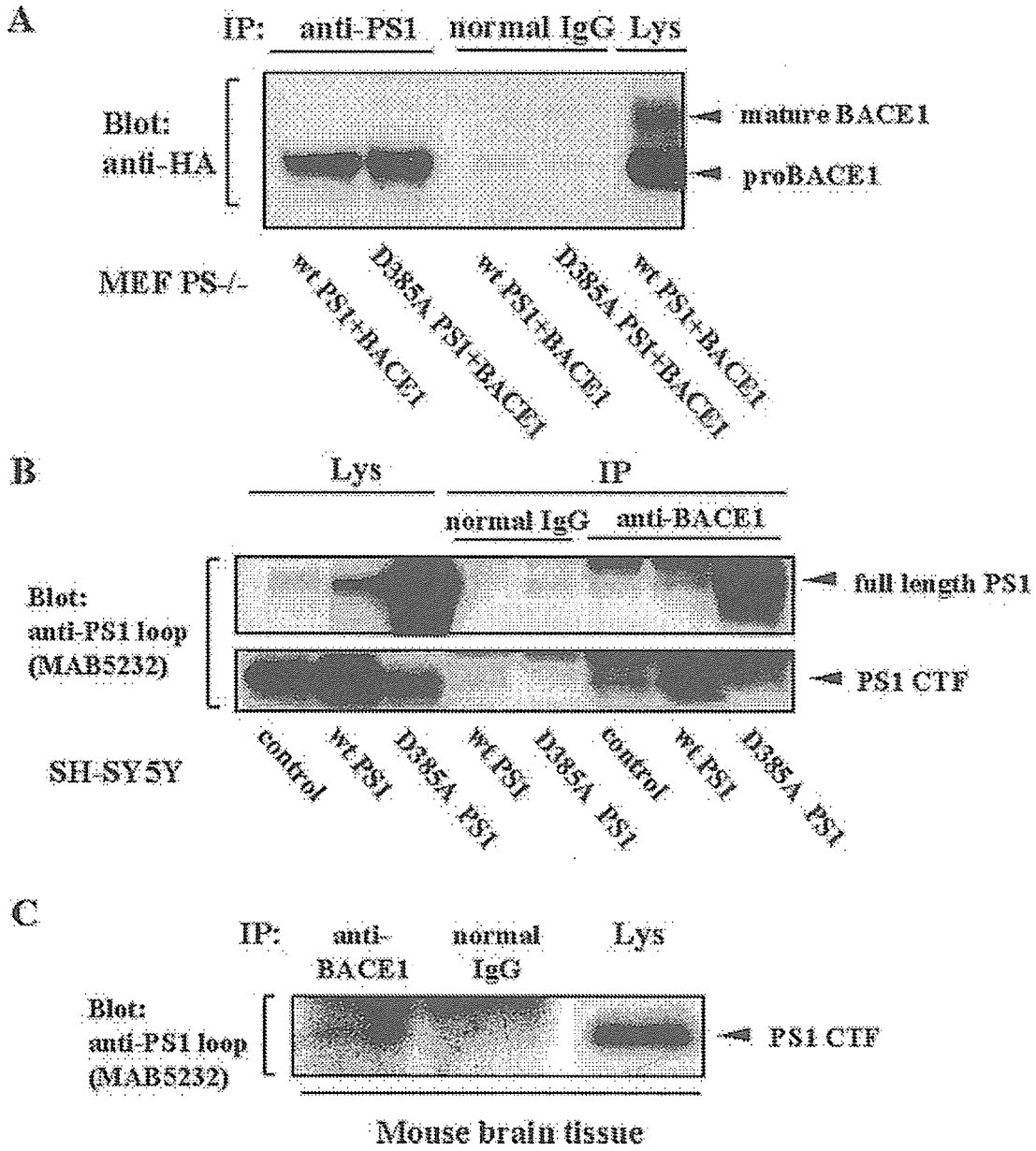

Fig. 4. PS1 and BACE1 physically interact with each other. **A:** HA-tagged BACE1 and either wt PS1 or D385A PS1 were transiently cotransfected into PS−/− MEFs. Each cell lysate was immunoprecipitated with anti-PS1 antibody against the N terminus. The cell lysate (Lys) as well as the immunoprecipitates (IP) were subjected to Western blotting with anti-HA antibody. ProBACE1, but not mature BACE1, was co-immunoprecipitated with either wt PS1 or D385A PS1. Almost no BACE1 immunoreactivity was observed from the samples of normal rabbit IgG used as negative controls. **B:** Equal amounts of cell lysates obtained from each SH-SY5Y cell line were immunoprecipitated using the anti-BACE1 antibody against the C terminus (Calbiochem), followed by Western blotting with the MAB5232 antibody against the loop domain of PS1. More PS1 C-terminal fragment (CTF) immunoreactivity was detected in wt PS1 cells (lane 4) than in control cells (lane 5). In D385A PS1 cells, almost no PS1 CTF bound to BACE1 was observed (lane 8: lower panel), reflecting the diminished endoproteolysis of D385A PS1 (lane 3). Conversely, solid association between full-length D385A PS1 and BACE1 was observed (lane 8: upper panel). Note that full-length wt PS1 was also associated with BACE1 in wt PS1 cells (lane 8: upper panel). No PS1 immunoreactivity was observed from the samples of normal rabbit IgG used as negative controls (lanes 5,6). **C:** Equal amounts of cell lysates obtained from adult mouse brain tissue were immunoprecipitated using the anti-BACE1 antibody (Calbiochem), followed by Western blotting using the MAB5232 antibody against the loop domain of PS1. PS1 CTF immunoreactivity was detected in the immunoprecipitates with the anti-BACE1 antibody (Calbiochem), whereas no PS1 CTF immunoreactivity was observed in the samples with normal rabbit IgG.

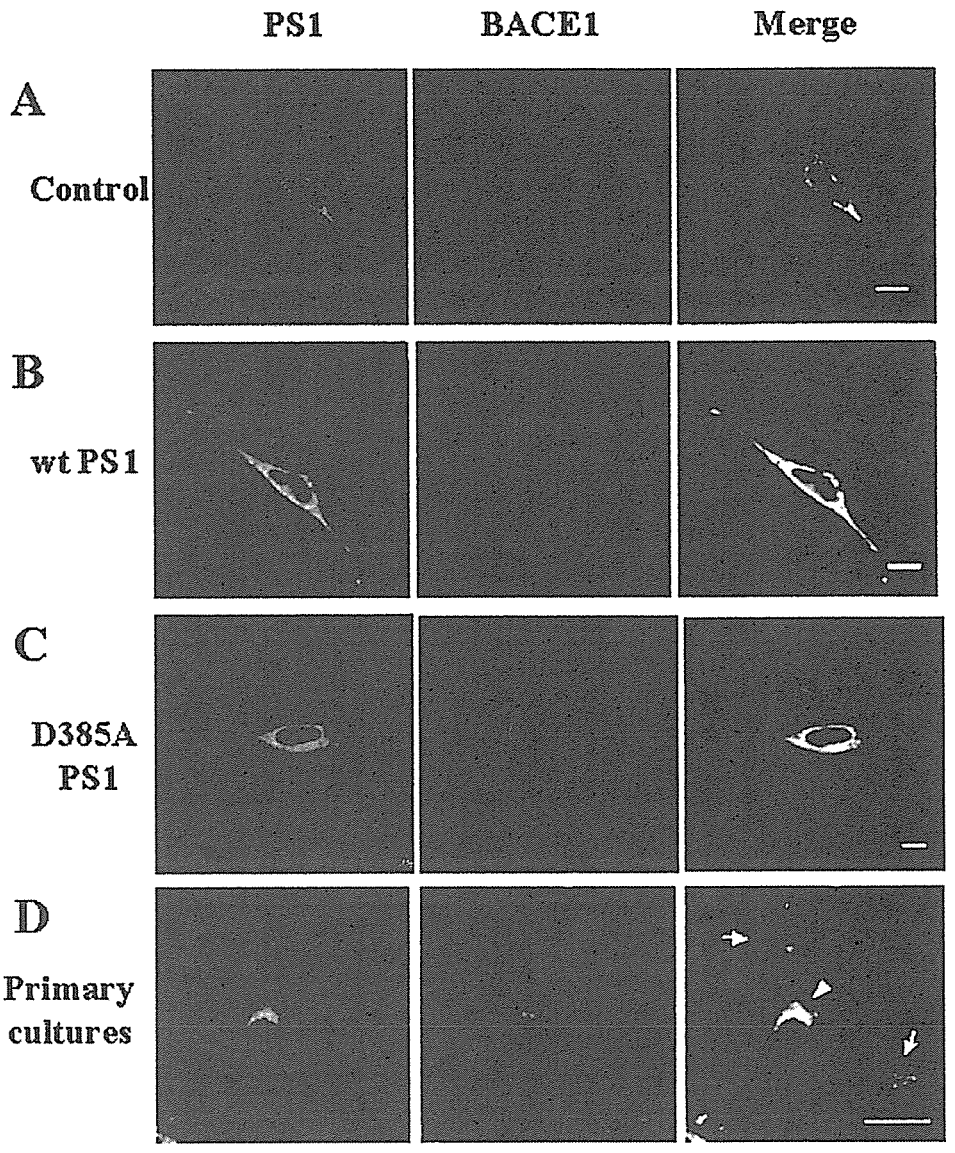

Fig. 5. PS1 and BACE1 colocalization in the SH-SY5Y cells and primary neurons. Each SH-SY5Y cell line (**A–C**) and rat primary cultured cortical neurons (**D**) were doubly stained with anti-BACE1 antibody against the C terminus (MAB5308) and anti-PS1 antibody against the N terminus. In each SH-SY5Y cell line, PS1 was largely colocalized with endogenous BACE1 (A–C, merged images). Note that an increase in wt PS1 immunoreactivity was accompanied by an increase in endogenous BACE1 immunoreactivity (A,B). Endogenous PS1 and BACE1 were considerably colocalized in a primary neuron, especially in a perinuclear area (arrowhead), compared to glial cells (arrows) (D, merged image). Scale bar = 20 μm.

anti-PS1 antibody against the N terminus and the MAB5308 antibody. As shown in Figure 5D, endogenous PS1 and BACE1 were considerably colocalized in a primary neuron, especially in a perinuclear area (arrowhead), compared to glial cells (arrows).

BACE1 in D385A PS1 Cells Fails to be Properly Transported From the ER to the Golgi

As shown in Figures 4 and 5, D385A PS1 is associated with endogenous BACE1 as well as wt PS1 in the immunoprecipitation and immunofluorescent experiments. However, BACE1 maturation is markedly downregulated in D385A PS1 cells in contrast to in wt PS1 cells (Fig. 2C). Because BACE1 undergoes trafficking-dependent maturation through the secretory pathway from the ER to the Golgi, we hypothesized that the transport of endogenous BACE1 from the ER to the Golgi was suppressed significantly in D385A PS1 cells. We first examined the intracellular localization of BACE1 in wt and D385A PS1 cells by immunofluorescent study using markers specific for the ER and the Golgi. Each cell line was double stained with the MAB5308 antibody to visualize BACE1 and either the anti-calnexin antibody to visualize the ER or the anti-mannosidase II antibody to visualize the Golgi. Interestingly, we found that a part of BACE1 in wt PS1 cells was apparently colocalized with mannosidase II in the perinuclear area (Fig. 6A, arrowhead), whereas the colocalization was negligible in D385A PS1 cells (Fig. 6B). Moreover, in D385A PS1 cells, most of BACE1 was colocalized with calnexin, a marker for the ER (Fig. 6C). These results suggest that proper transport of BACE1 from the ER to the

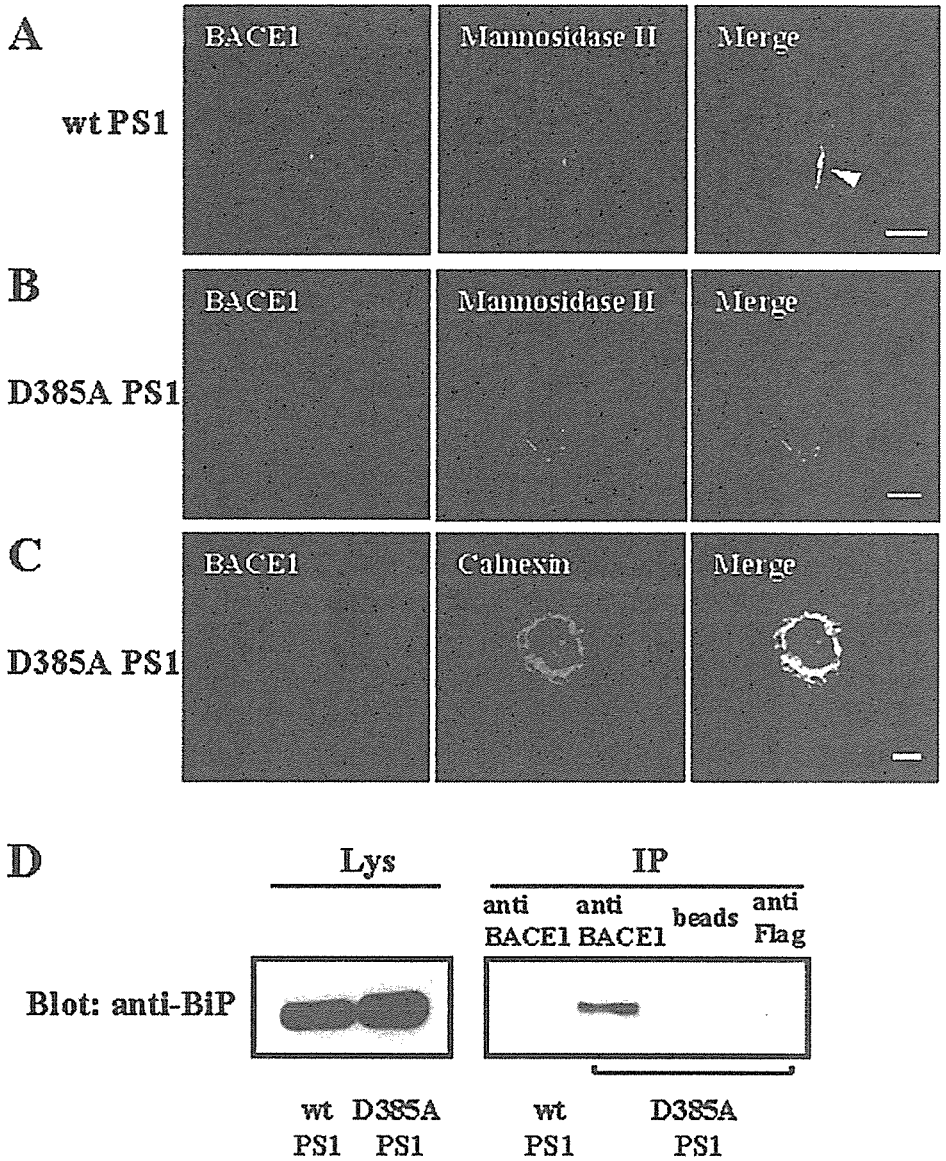

Fig. 6. Endogenous BACE1 in D385A PS1 cells is largely retained in the ER and fails to be transported to the Golgi. **A,B:** Wt PS1 cells and D385A PS1 cells were doubly stained with anti-BACE1 antibody against the C terminus (MAB5308) and anti-mannosidase II antibody. No apparent colocalization of endogenous BACE1 with mannosidase II, a marker for the Golgi, was observed in D385A PS1 cells (B), whereas endogenous BACE1 in wt PS1 cells was partially colocalized with mannosidase II (A, arrowhead). **C:** D385A PS1 cells were doubly stained with anti-BACE1 antibody (MAB5308) and anti-calnexin antibody. Endogenous BACE1 in D385A PS1 cells was colocalized mostly with calnexin, a marker for the ER (C, merged image). Scale bar = 20 μm. **D:** Equal amounts of whole cell lysates from wt PS1 and D385A PS1 cells were immunoprecipitated with anti-BACE1 antibody (MAB5308). Cell lysate (Lys) as well as immunoprecipitates (IP) were subjected to immunoblotting with anti-BiP antibody. The immunoprecipitates from D385A PS1 cell lysate showed BiP immunoreactivity. No BiP immunoreactivity was observed in the immunoprecipitate from the wt PS1 cell lysate, or from the samples of Protein G-Sepharose beads alone (beads) or anti-Flag antibody, used as negative controls.

Golgi is impaired in D385A PS1 cells, and are compatible with the previous observation that BACE1 maturation is downregulated in D385A PS1 (Fig. 2C).

BiP, an ER-resident molecular chaperone, binds to misfolded, underglycosylated, or unassembled proteins and assists with protein folding and retention of misfolded proteins in the ER (Gething, 1999). We examined the possibility that BACE1 in D385A PS1 cells, which might become terminally misfolded after release from the ER folding machinery, was preferentially associated with BiP. Equal amounts of cell lysate obtained from either wt PS1 or D385A PS1 cells were immunoprecipitated using the MAB5308 antibody, and the immunoprecipitate was subjected to Western blotting using an anti-BiP antibody. The immunoreactivity of BiP co-immunoprecipitated with BACE1 was observed in D385A PS1 cells, whereas it was not detected in wt PS1 cells (Fig. 6D).

These results suggest that proper transport of endogenous BACE1 from the ER to the Golgi is impaired in D385A PS1 cells, resulting in aberrant retention of BACE1 within the ER, and its association with BiP as unfolded or misfolded proteins.

DISCUSSION

Despite of extensive research, the pathogenesis of AD is still in an enigma. Several recent reports showed elevated β-secretase expression and enzymatic activity in the absence of the alteration of message expression in AD brains (Fukumoto et al., 2002; Holsinger et al., 2002; Yang et al., 2003), indicating the dysregulation of β-secretase activity may be involved in AD pathogenesis. Interestingly, amino-terminally truncated Aβ peptides, which are known to be β-secretase cleavage products, were more abundant in

the brains of subjects carrying PS1 gene mutations causing FAD than in those with sporadic AD and FAD associated with a point mutation in APP gene (Russo et al., 2000), indicating that FAD-linked mutations in PS1 can somehow affect β-secretase activity. However, the functional link between PS1 and BACE1 has never been elucidated, although they are supposed to be the 'key players' of AD pathogenesis.

In the present study, we showed a solid evidence for a novel function of PS1 in regulating BACE1 maturation. The levels of mature BACE1 either endogenously or exogenously expressed in PS−/− MEFs were reduced significantly, as compared to that in wt MEFs. These results suggest that the presence of presenilins can promote BACE1 maturation. To validate this effect of PS1 in neuronal cells endogenously expressing BACE1, we analyzed stably transfected SH-SY5Y cells with either wt PS1 or dominant-negative (D385A) PS1. Interestingly, the overexpression of D385A PS1 decreased the level of mature BACE1 protein by 50%, accompanied by a 60% reduction in the ratio of mature:proBACE1 as compared to control cells. Conversely, the overexpression of wt PS1 upregulated the level of mature BACE1 protein. Given that the levels of BACE1 mRNA were comparable between wt PS1 and D385A PS1 cells, these results indicate that functional PS1 positively regulates BACE1 maturation post-translationally.

Intriguingly, a recent study showed that targeting BACE1 to lipid rafts, cholesterol- and sphingolipid-enriched microdomains within cellular membranes, upregulated the β-site processing of APP, leading to a drastic increase in Aβ generation in SH-SY5Y cells (Cordy et al., 2003), indicating that proper distribution of BACE1 is crucially important for regulating Aβ generation. Although a growing number of evidence has strongly supported a direct role for PS1 in the γ-secretase cleavage of APP as the catalytic component of the γ-secretase complex (Wolfe et al., 1999a,b), a function of PS1 in protein trafficking has also been shown, especially with regard to APP and nicastrin (Kim et al., 2001; Edbauer et al., 2002; Leem et al., 2002a,b; Cai et al., 2003; Herreman et al., 2003). This function is consistent with a functional analogy to the weakly homologous SPE4 protein of *C. elegans*, which has been implicated in the maintenance of a Golgi-derived membranous organelle and is thought to be important in the partitioning of protein and cell membrane products in maturing spermatocytes (L'Hernault and Arduengo, 1992). These previous findings provide support for the idea that PS1 may regulate BACE1 trafficking, thereby modulating its maturation.

Indeed, we found that BACE1 in D385A PS1 cells was mostly retained within the ER and was negligibly localized within the Golgi (Fig. 6B,C), whereas a part of BACE1 in wt PS1 cells was apparently localized within the Golgi (Fig. 6A). Moreover, we found that BACE1 in D385A PS1 cells was associated significantly with BiP, an ER resident molecular chaperone, in contrast to in wt PS1 cells (Fig. 6D), presumably attributable to its aberrant retention within the ER. Interestingly, a splice variant of BACE1, lacking terminal two-thirds of exon 3, is expressed in pancreas. This isoform of BACE1, lacking β-secretase activity, colocalizes with BiP and its transport along the secretory pathway is blocked at the level of the ER, indicating that misfolded or non-functional BACE1 can associate with BiP in the ER (Bodendorf et al., 2001). These results indicate that wt PS1 upregulates BACE1 maturation, whereas the absence of PS1 or non-functional D385A PS1 downregulates its maturation as a result of its inefficient transport from the ER to the Golgi.

The above data raises the question whether PS1/γ-secretase activity directly affects the trafficking and maturation of BACE1 or not. We observed no significant effect of the γ-secretase inhibitors on BACE1 maturation in primary neurons. Thus, we consider that PS1/γ-secretase activity itself is less likely to be involved in the maturation process of BACE1. Nevertheless, further experiments will be needed to elucidate a relationship between the PS1/γ-secretase activity and the novel function of PS1 in the trafficking and maturation of BACE1.

Finally, how dose PS1 regulate BACE1 trafficking and maturation? Although this question was not clarified in the present study, it was reported recently that PS1 and BACE1 are transported in the same membrane vesicles along the axons *in vivo*, via the direct binding of APP to the kinesin light chain subunit of kinesin-I, a microtubule motor protein (Kamal et al., 2001). Moreover, it was also shown that PS1 and nicastrin, the major components of the γ-secretase complex, interact with BACE1, suggesting that they may regulate β-secretase activity via the interaction with BACE1 (Hattori et al., 2002; Hebert et al., 2003). Consistent with these reports, we showed PS1-BACE1 interaction in the cell lines, primary neurons, and brain tissue and found that PS1 interacted preferably with proBACE1 rather than mature BACE1. Interestingly, we observed the solid binding between D385A PS1 and proBACE1. Although we cannot clarify a mechanism how D385A PS1 downregulates BACE1 maturation despite the solid interaction in the present study, one explanation is that the transport of proBACE1 to the Golgi after the interaction in the ER can be a process required for BACE1 maturation. We think there is a possibility that D385A PS1 is defective in this trafficking function, although the solid interaction with proBACE1 occurs in the ER. Taken together, PS1 may directly be involved in BACE1 maturation via stabilizing proBACE1 or promoting its efficient transport from the ER to the Golgi, although further experiments are needed to elucidate this mechanism.

In summary, our results show that PS1 is involved significantly in BACE1 maturation. This finding, for the first time, provided us the solid link between β- and γ-secretase. From observations obtained from the present study, we would like to extend our view of PS1 function further, and suggest that PS1 contributes to the dual regulation of β- and γ-secretase by regulating the intracellular trafficking of β-secretase and acting as a key component of γ-secretase. Consequently, PS1 may determine the magnitude of amyloidogenic processing of APP, thereby

contributing to the amyloid pathology. Although the regulatory mechanisms remain unknown, aberrant trafficking function of PS1 may lead to increased Aβ generation, and may underlie the pathogenesis of AD. In a future study, it will be significant to investigate effects of the clinical PS1 mutations or lipid raft on the novel function of PS1 in the intracellular trafficking of BACE1.

ACKNOWLEDGMENTS

We sincerely thank to Dr. De Strooper and Dr. Saftig for providing wt and PS−/− MEF cell lines. We also thank Dr. Kinoshita for helpful discussions.

REFERENCES

Annaert WG, Esselens C, Baert V, Boeve C, Snellings G, Cupers P, Craessaerts K, De Strooper B. 2001. Interaction with telencephalon and the amyloid precursor protein predicts a ring structure for presenilins. Neuron 32:579–589.

Armogida M, Petit A, Vincent B, Scarzello S, da Costa CA, Checler F. 2001. Endogenous beta-amyloid production in presenilin-deficient embryonic mouse fibroblasts. Nat Cell Biol 3:1030–1033.

Bodendorf U, Fischer F, Bodian D, Multhaup G, Paganetti P. 2001. A splice variant of beta-secretase deficient in the amyloidogenic processing of the amyloid precursor protein. J Biol Chem 276:12019–12023.

Borchelt DR, Thinakaran G, Eckman CB, Lee MK, Davenport F, Ratovitsky T, Prada CM, Kim G, Seekins S, Yager D, Slunt HH, Wang R, Seeger M, Levey AI, Gandy SE, Copeland NG, Jenkins NA, Price DL, Younkin SG, Sisodia SS. 1996. Familial Alzheimer's disease-linked presenilin 1 variants elevate Abeta1-42/1-40 ratio in vitro and in vivo. Neuron 17:1005–1013.

Bradford MM. 1976. A rapid and sensitive method for the quantitation of microgram quantities of protein utilizing the principle of protein-dye binding. Anal Biochem 72:248–254.

Cai D, Leem JY, Greenfield JP, Wang P, Kim BS, Wang R, Lopes KO, Kim SH, Zheng H, Greengard P, Sisodia SS, Thinakaran G, Xu H. 2003. Presenilin-1 regulates intracellular trafficking and cell surface delivery of beta-amyloid precursor protein. J Biol Chem 278:3446–3454.

Capell A, Grunberg J, Pesold B, Diehlmann A, Citron M, Nixon R, Beyreuther K, Selkoe DJ, Haass C. 1998. The proteolytic fragments of the Alzheimer's disease-associated presenilin-1 form heterodimers and occur as a 100-150-kDa molecular mass complex. J Biol Chem 273: 3205–3211.

Capell A, Steiner H, Willem M, Kaiser H, Meyer C, Walter J, Lammich S, Multhaup G, Haass C. 2000. Maturation and pro-peptide cleavage of beta-secretase. J Biol Chem 275:30849–30854.

Cordy JM, Hussain I, Dingwall C, Hooper NM, Turner AJ. 2003. Exclusively targeting beta-secretase to lipid rafts by GPI-anchor addition up-regulates beta-site processing of the amyloid precursor protein. Proc Natl Acad Sci U S A 100:11735–11740.

Creemers JW, Ines Dominguez D, Plets E, Serneels L, Taylor NA, Multhaup G, Craessaerts K, Annaert W, De Strooper B. 2001. Processing of beta-secretase by furin and other members of the proprotein convertase family. J Biol Chem 276:4211–4217.

Duff K, Eckman C, Zehr C, Yu X, Prada CM, Perez-tur J, Hutton M, Buee L, Harigaya Y, Yager D, Morgan D, Gordon MN, Holcomb L, Refolo L, Zenk B, Hardy J, Younkin S. 1996. Increased amyloid-beta42(43) in brains of mice expressing mutant presenilin 1. Nature 383: 710–713.

Edbauer D, Winkler E, Haass C, Steiner H. 2002. Presenilin and nicastrin regulate each other and determine amyloid beta-peptide production via complex formation. Proc Natl Acad Sci U S A 99:8666–8671.

Francis R, McGrath G, Zhang J, Ruddy DA, Sym M, Apfeld J, Nicoll M, Maxwell M, Hai B, Ellis MC, Parks AL, Xu W, Li J, Gurney M, Myers RL, Himes CS, Hiebsch R, Ruble C, Nye JS, Curtis D. 2002. aph-1 and pen-2 are required for Notch pathway signaling, gamma-secretase cleavage of betaAPP, and presenilin protein accumulation. Dev Cell 3:85–97.

Fukumoto H, Cheung BS, Hyman BT, Irizarry MC. 2002. Beta-secretase protein and activity are increased in the neocortex in Alzheimer disease. Arch Neurol 59:1381–1389.

Gething MJ. 1999. Role and regulation of the ER chaperone BiP. Semin Cell Dev Biol 10:465–72.

Golde TE, Cai XD, Shoji M, Younkin SG. 1993. Production of amyloid beta protein from normal amyloid beta-protein precursor (beta APP) and the mutated beta APPS linked to familial Alzheimer's disease. Ann N Y Acad Sci 695:103–108.

Gu Y, Chen F, Sanjo N, Kawarai T, Hasegawa H, Duthie M, Li W, Ruan X, Luthra A, Mount HT, Tandon A, Fraser PE, St George-Hyslop P. 2003. APH-1 interacts with mature and immature forms of presenilins and nicastrin and may play a role in maturation of presenilin:nicastrin complexes. J Biol Chem 278:7374–7380.

Haass C, Hung AY, Schlossmacher MG, Oltersdorf T, Teplow DB, Selkoe DJ. 1993. Normal cellular processing of the beta-amyloid precursor protein results in the secretion of the amyloid beta peptide and related molecules. Ann N Y Acad Sci 695:109–116.

Haniu M, Denis P, Young Y, Mendiaz EA, Fuller J, Hui JO, Bennett BD, Kahn S, Ross S, Burgess T, Katta V, Rogers G, Vassar R, Citron M. 2000. Characterization of Alzheimer's beta-secretase protein BACE. A pepsin family member with unusual properties. J Biol Chem 275:21099–21106.

Hardy J. 1997a. The Alzheimer family of diseases: many etiologies, one pathogenesis? Proc Natl Acad Sci U S A 94:2095–2097.

Hardy J. 1997b. Amyloid, the presenilins and Alzheimer's disease. Trends Neurosci 20:154–159.

Hattori C, Asai M, Oma Y, Kino Y, Sasagawa N, Saido TC, Maruyama K, Ishiura S. 2002. BACE1 interacts with nicastrin. Biochem Biophys Res Commun 293:1228–1232.

Hebert SS, Bourdages V, Godin C, Ferland M, Carreau M, Levesque G. 2003. Presenilin-1 interacts directly with the beta-site amyloid protein precursor cleaving enzyme (BACE1). Neurobiol Dis 13:238–245.

Herreman A, Hartmann D, Annaert W, Saftig P, Craessaerts K, Serneels L, Umans L, Schrijvers V, Checler F, Vanderstichele H, Baekelandt V, Dressel R, Cupers P, Huylebroeck D, Zwijsen A, Van Leuven F, De Strooper B. 1999. Presenilin 2 deficiency causes a mild pulmonary phenotype and no changes in amyloid precursor protein processing but enhances the embryonic lethal phenotype of presenilin 1 deficiency. Proc Natl Acad Sci U S A 96:11872–11877.

Herreman A, Van Gassen G, Bentahir M, Nyabi O, Craessaerts K, Mueller U, Annaert W, De Strooper B. 2003. gamma-Secretase activity requires the presenilin-dependent trafficking of nicastrin through the Golgi apparatus but not its complex glycosylation. J Cell Sci 116:1127–1136.

Holsinger RM, McLean CA, Beyreuther K, Masters CL, Evin G. 2002. Increased expression of the amyloid precursor beta-secretase in Alzheimer's disease. Ann Neurol 51:783–786.

Huse JT, Pijak DS, Leslie GJ, Lee VM, Doms RW. 2000. Maturation and endosomal targeting of beta-site amyloid precursor protein-cleaving enzyme. The Alzheimer's disease beta-secretase. J Biol Chem 275:33729–33737.

Hussain I, Powell D, Howlett DR, Tew DG, Meek TD, Chapman C, Gloger IS, Murphy KE, Southan CD, Ryan DM, Smith TS, Simmons DL, Walsh FS, Dingwall C, Christie G. 1999. Identification of a novel aspartic protease (Asp 2) as beta-secretase. Mol Cell Neurosci 14:419–427.

Kamal A, Almenar-Queralt A, LeBlanc JF, Roberts EA, Goldstein LS. 2001. Kinesin-mediated axonal transport of a membrane compartment containing beta-secretase and presenilin-1 requires APP. Nature 414: 643–648.

Kang J, Lemaire HG, Unterbeck A, Salbaum JM, Masters CL, Grzeschik KH, Multhaup G, Beyreuther K, Muller-Hill B. 1987. The precursor of Alzheimer's disease amyloid A4 protein resembles a cell-surface receptor. Nature 325:733–736.

Kihara T, Shimohama S, Sawada H, Kimura J, Kume T, Kochiyama H, Maeda T, Akaike A. 1997. Nicotinic receptor stimulation protects neurons against beta-amyloid toxicity. Ann Neurol 42:159–163.

Kim SH, Leem JY, Lah JJ, Slunt HH, Levey AI, Thinakaran G, Sisodia SS. 2001. Multiple effects of aspartate mutant presenilin 1 on the processing and trafficking of amyloid precursor protein. J Biol Chem 276:43343–43350.

L'Hernault SW, Arduengo PM. 1992. Mutation of a putative sperm membrane protein in Caenorhabditis elegans prevents sperm differentiation but not its associated meiotic divisions. J Cell Biol 119:55–68.

Lee SF, Shah S, Li H, Yu C, Han W, Yu G. 2002. Mammalian APH-1 interacts with presenilin and nicastrin and is required for intramembrane proteolysis of amyloid-beta precursor protein and Notch. J Biol Chem 277:45013–45019.

Leem JY, Saura CA, Pietrzik C, Christianson J, Wanamaker C, King LT, Veselits ML, Tomita T, Gasparini L, Iwatsubo T, Xu H, Green WN, Koo EH, Thinakaran G. 2002a. A role for presenilin 1 in regulating the delivery of amyloid precursor protein to the cell surface. Neurobiol Dis 11:64–82.

Leem JY, Vijayan S, Han P, Cai D, Machura M, Lopes KO, Veselits ML, Xu H, Thinakaran G. 2002b. Presenilin 1 is required for maturation and cell surface accumulation of nicastrin. J Biol Chem 277:19236–19240.

Naruse S, Thinakaran G, Luo JJ, Kusiak JW, Tomita T, Iwatsubo T, Qian X, Ginty DD, Price DL, Borchelt DR, Wong PC, Sisodia SS. 1998. Effects of PS1 deficiency on membrane protein trafficking in neurons. Neuron 21:1213–1221.

Pinnix I, Council JE, Roseberry B, Onstead L, Mallender W, Sucic J, Sambamurti K. 2001. Convertases other than furin cleave beta-secretase to its mature form. FASEB J 15:18101812.

Rogaev EI, Sherrington R, Rogaeva EA, Levesque G, Ikeda M, Liang Y, Chi H, Lin C, Holman K, Tsuda T, et al. 1995. Familial Alzheimer's disease in kindreds with missense mutations in a gene on chromosome 1 related to the Alzheimer's disease type 3 gene. Nature 376:775–778.

Russo C, Schettini G, Saido TC, Hulette C, Lippa C, Lannfelt L, Ghetti B, Gambetti P, Tabaton M, Teller JK. 2000. Presenilin-1 mutations in Alzheimer's disease. Nature 405:531–532.

Sherrington R, Rogaev EI, Liang Y, Rogaeva EA, Levesque G, Ikeda M, Chi H, Lin C, Li G, Holman K, et al. 1995. Cloning of a gene bearing missense mutations in early-onset familial Alzheimer's disease. Nature 375:754–760.

Sinha S, Anderson JP, Barbour R, Basi GS, Caccavello R, Davis D, Doan M, Dovey HF, Frigon N, Hong J, Jacobson-Croak K, Jewett N, Keim P, Knops J, Lieberburg I, Power M, Tan H, Tatsuno G, Tung J, Schenk D, Seubert P, Suomensaari SM, Wang S, Walker D, Zhao J, McConlogue L, John V. 1999. Purification and cloning of amyloid precursor protein beta-secretase from human brain. Nature 402:537–540.

Steiner H, Winkler E, Edbauer D, Prokop S, Basset G, Yamasaki A, Kostka M, Haass C. 2002. PEN-2 is an integral component of the gamma-secretase complex required for coordinated expression of presenilin and nicastrin. J Biol Chem 277:39062–39065.

Thinakaran G. 1999. The role of presenilins in Alzheimer's disease. J Clin Invest 104:1321–1327.

Uemura K, Kihara T, Kuzuya A, Okawa K, Nishimoto T, Ninomiya H, Sugimoto H, Kinoshita A, Shimohama S. 2006. Characterization of sequential N-cadherin cleavage by ADAM10 and PS1. Neurosci Lett 402:278–283.

Uemura K, Kitagawa N, Kohno R, Kuzuya A, Kageyama T, Chonabayashi K, Shibasaki H, Shimohama S. 2003a. Presenilin 1 is involved in maturation and trafficking of N-cadherin to the plasma membrane. J Neurosci Res 74:184–191.

Uemura K, Kitagawa N, Kohno R, Kuzuya A, Kageyama T, Shibasaki H, Shimohama S. 2003b. Presenilin 1 mediates retinoic acid-induced differentiation of SH-SY5Y cells through facilitation of Wnt signaling. J Neurosci Res 73:166–175.

Vassar R, Bennett BD, Babu-Khan S, Kahn S, Mendiaz EA, Denis P, Teplow DB, Ross S, Amarante P, Loeloff R, Luo Y, Fisher S, Fuller J, Edenson S, Lile J, Jarosinski MA, Biere AL, Curran E, Burgess T, Louis JC, Collins F, Treanor J, Rogers G, Citron M. 1999. Beta-secretase cleavage of Alzheimer's amyloid precursor protein by the transmembrane aspartic protease BACE. Science 286:735–741.

Walter J, Fluhrer R, Hartung B, Willem M, Kaether C, Capell A, Lammich S, Multhaup G, Haass C. 2001. Phosphorylation regulates intracellular trafficking of beta-secretase. J Biol Chem 276:14634–14641.

Wilson CA, Doms RW, Zheng H, Lee VM. 2002. Presenilins are not required for A beta 42 production in the early secretory pathway. Nat Neurosci 5:849–855.

Wolfe MS, De Los Angeles J, Miller DD, Xia W, Selkoe DJ. 1999a. Are presenilins intramembrane-cleaving proteases? Implications for the molecular mechanism of Alzheimer's disease. Biochemistry 38:11223–11230.

Wolfe MS, Xia W, Ostaszewski BL, Diehl TS, Kimberly WT, Selkoe DJ. 1999b. Two transmembrane aspartates in presenilin-1 required for presenilin endoproteolysis and gamma-secretase activity. Nature 398:513–517.

Yan R, Bienkowski MJ, Shuck ME, Miao H, Tory MC, Pauley AM, Brashier JR, Stratman NC, Mathews WR, Buhl AE, Carter DB, Tomasselli AG, Parodi LA, Heinrikson RL, Gurney ME. 1999. Membrane-anchored aspartyl protease with Alzheimer's disease beta-secretase activity. Nature 402:533–537.

Yang LB, Lindholm K, Yan R, Citron M, Xia W, Yang XL, Beach T, Sue L, Wong P, Price D, Li R, Shen Y. 2003. Elevated beta-secretase expression and enzymatic activity detected in sporadic Alzheimer disease. Nat Med 9:3–4.

Yu G, Nishimura M, Arawaka S, Levitan D, Zhang L, Tandon A, Song YQ, Rogaeva E, Chen F, Kawarai T, Supala A, Levesque L, Yu H, Yang DS, Holmes E, Milman P, Liang Y, Zhang DM, Xu DH, Sato C, Rogaev E, Smith M, Janus C, Zhang Y, Aebersold R, Farrer LS, Sorbi S, Bruni A, Fraser P, St George-Hyslop P. 2000. Nicastrin modulates presenilin-mediated notch/glp-1 signal transduction and betaAPP processing. Nature 407:48–54.

Human Molecular Genetics, 2007, Vol. 16, No. 1 **50–60**
doi:10.1093/hmg/ddl439
Advance Access published on November 20, 2006

Pael receptor induces death of dopaminergic neurons in the substantia nigra via endoplasmic reticulum stress and dopamine toxicity, which is enhanced under condition of parkin inactivation

Yasuko Kitao[1,*,†], Yuzuru Imai[2,†], Kentaro Ozawa[1], Ayane Kataoka[2], Toshio Ikeda[3], Mariko Soda[2], Kazuhiko Nakimawa[4], Hiroshi Kiyama[4], David M. Stern[7], Osamu Hori[1], Kazumasa Wakamatsu[6], Shosuke Ito[6], Shigeyoshi Itohara[3], Ryosuke Takahashi[2,5,†] and Satoshi Ogawa[1,†]

[1]Department of Neuroanatomy, Kanazawa University Medical School, 13-1, Takara-machi, Kanazawa City, 920-8640 Ishikawa, Japan, [2]Laboratory for Motor System Neurodegeneration and [3]Laboratory for Behavioral Genetics and RIKEN Brain Science Institute (BSI), Saitama 351-0198, Japan, [4]Department of Anatomy and Neurobiology, Osaka City University, Graduate School of Medicine, Osaka, Japan, [5]Department of Neurology, Kyoto University Medical School, Kyoto, Japan, [6]Department of Chemistry, Fujita Health University School of Health Sciences, Aichi 470-1192, Japan and [7]Dean's Office, College of Medicine, University of Cincinnati, Cincinnati, OH 45267, USA

Received August 2, 2006; Revised October 19, 2006; Accepted November 13, 2006

Selective loss of dopaminergic neurons is the final common pathway in Parkinson's disease. Expression of Parkin associated endothelin-receptor like receptor (Pael-R) in mouse brain was achieved by injecting adenoviral vectors carrying a modified neuron-specific promoter and Cre recombinase into the striatum. Upregulation of Pael-R in the substantia nigra pars compacta of mice by retrograde infection induced endoplasmic reticulum (ER) stress leads to death of dopaminergic neurons. The role of ER stress in dopaminergic neuronal vulnerability was highlighted by their decreased survival in mice deficient in the ubiquitin-protein ligase Parkin and the ER chaperone ORP150 (150 kDa oxygen-regulated protein). Dopamine-related toxicity was also a key factor, as a dopamine synthesis inhibitor blocked neuronal death in parkin null mice. These data suggest a model in which ER- and dopamine-related stress are major contributors to decreased viability of dopaminergic neurons in a setting relevant to Parkinson's disease.

INTRODUCTION

Though Parkinson's disease (PD) is a major contributor to disability and death in the aging population, the molecular basis of selective dopaminergic neuronal toxicity is still under investigation. Progression of the clinical syndrome associated with PD, which includes a well-characterized movement disorder, correlates closely with inexorable loss of neurons in the substantia nigra pars compacta (SNpc) (1).

Mutations in the *Parkin* gene (2) have been identified in the autosomal recessive form of PD (AR-JP), a major cause of juvenile PD. Parkin is a 465 amino acid polypeptide with properties of an ubiquitin-protein ligase (E3) whose N-terminus displays homology to ubiquitin and C-terminus is comprised of two RING fingers flanking a cysteine-rich domain, termed in between RING fingers (IBR) (3–5). Consistent with this view, AR-JP-linked parkin mutants are defective in E3 activity (6–8).

A putative G protein-coupled transmembrane polypeptide, Pael Receptor [Parkin-associated endothelin-receptor like receptor (Pael-R)], has been identified as a Parkin substrate (9). Expression of Pael-R in cultured cells results in accumulation

*To whom correspondence should be addressed. Tel: +81 762652162; Fax: +81 762344222; Email: kitao@nanat.m.kanazawa-u.ac.jp
†These authors equally contributed to this work.

of unfolded, insoluble and ubiquinated Pael-R in the ER, eventuating in ER stress, as indicated by upregulation of chaperones, such as GRP78/BiP, and subsequent neuronal death (10). Overexpression of Parkin in this *in vitro* model resulted in removal/degradation of accumulated Pael-R and increased cell viability. The relevance of ER stress in the central nervous system to pathologic situations and normal neuronal development is suggested by induction of the unfolded protein response (UPR) in cell stress associated with cerebral ischemia (11,12) and exposure to excitatory amino acids (13), as well as during rapid neuronal growth in the neonatal period (14). Salient features of the UPR include upregulation of ER chaperones, suppression of general translation, and activation of the upiquitin-proteasome pathway.

A key facet of the pathology of PD is limitation of cell loss to dopaminergic neurons, especially in the SNpc. In this context, studies of Pael-R might be especially relevant. Pan-neuronal expression of Pael-R in *Drosophila* brain caused selective, age-dependent degeneration of dopaminergic neurons (10). Thus, increased levels of Pael-R render dopaminergic neurons vulnerable to cell death. In the current study, we have found that increased expression of Pael-R in mice in the SNpc results in neuronal death which is accentuated by suppression of Parkin (in $Parkin^{-/-}$ mice) or an ER chaperone (in $Orp150^{+/-}$ mice). In contrast, a dopamine (DA) synthesis inhibitor had neuroprotective properties in this system. Thus, we propose a unified model for cytotoxicity in PD through which a combination of ER stress and dopamine toxicity, potentially acting in concert with mitochondrial dysfunction, result in an ascending cycle of cellular perturbation and, ultimately, death of dopaminergic neurons.

RESULTS

Retrograde and neuron-specific gene expression by adenoviral vectors in the SNpc

It was essential to develop a system with cell-specific protein expression which could be targeted to the SNpc. For this purpose, we established two adenoviral vectors in which nuclear Cre-recombinase was driven by cell-specific promoters; for neuronal expression, we employed AxS2NPNCre (abbreviated as S2NPNCre) with a modified SCG10 promoter (superior cervical ganglia neural-specific 10 protein), and for glial-specific expression, we utilized AxGFAPNCre (abbreviated as GFAPNCre) with the glial fibrillary acidic protein promoter (Fig. 1A). When either of these adenoviral vectors was co-infected with AxCALNLEGFP (abbreviated as LoxEGFP), specific expression of EGFP occurred in neurons (with S2NPNCre) or astrocytes (with GFAPNCre) in a cell culture system (not shown). *In vivo*expression studies were performed in mice by co-infecting either S2NPNCre with LoxEGFP, or GFAPNCre with LoxEGFP. Spatial limitation of gene expression was achieved by injecting viral vectors into the striatum (Fig. 1B), resulting in expression of EGFP protein in the ipsilateral SNpc (Fig. 1C, top panel). When S2NPNCre was injected with LoxEGFP, expression of EGFP (marking neurons) and tyrosine hydroxylase [TH; marking dopaminergic neurons in the SNpc (15)] overlapped (Fig. 1C; middle set of panels); quantitation of this overlap by image analysis, based on studying multiple fields, confirmed extensive coexpression of EGFP with TH (Fig. 1D). In contrast, there was no overlap of EGFP, following injection of S2NPNCre with LoxEGFP, when immunostaining was performed to visualize GFAP (Fig. 1C, lowest set of panels and Fig. 1D). These data indicate that co-infection of the striatum with recombinant adenoviral vectors encoding cell-specific Cre recombinase and EGFP (or other transgenes) flanked by lox P sites, leads to retrograde transport of adenovirus in the nigrostriatal system resulting in gene expression in the SNpc.

Expression of Pael-R in the SNpc activates the unfolded protein response

Using this adenoviral system, we sought to express Pael-R in the SNpc. For this purpose, an adenoviral vector was made with expression of Pael-R under control of the SCG10 promoter regulated by the LoxP system (16), AxCALNLPael-R (abbreviated as LoxPael-R; Fig. 2A). Co-injection of the two adenoviral vectors, S2NPNCre and LoxPael-R, into the striatum increased expression of Pael-R in the SNpc (Fig. 2B, referred to as ipsilateral side). Enhanced expression of Pael-R required both vectors to be co-injected, and was specific for neurons.

Based on previous *in vitro* findings, increased expression of Pael-R in dopaminergic neurons might result in ER stress and diminished cell viability (9). Control experiments were performed by co-injecting three adenoviral vectors, S2NPNCre, LoxEGFP and LoxLacZ, into the striatum on one side of the brain, referred to as contralateral (Fig. 2C, upper panels). Expression of an ER chaperone, ORP150 (oxygen-regulated protein 150), known to increase with ER stress (11), was assessed in neurons expressing EGFP (Fig. 2C, upper panels). ORP150 levels, assessed by Western blotting, were unchanged in the SNpc following injection of this combination of adenoviral vectors (Fig. 2D, left portion and Fig. 2E, middle panel, open bars). Faint ORP150 staining was demonstrated in multiple cells and a much stronger signal for EGFP was observed (Fig. 2C, upper panels). ORP150 has a putative ATPase domain and protein binding site, suggesting that it may have a chaperone-like role in maintaining ER function under stress [(17), and see below]. In this context, we have demonstrated that overexpression of ORP150 rescues neurons from cell death mediated by ischemia (11,12) and excitatory amino acids (13). When S2NPNCre, LoxEGFP and LoxPael-R were injected into the striatum on the ipsilateral side of the brain (the vectors with LoxLacZ in place of LoxPael-R were injected on the contralateral side), a prominent increase in Pael-R in the SNpc (Fig, 2D, right portion) was accompanied by increased expression of ORP150 (Fig. 2C, lower panels) in Pael-R expressing neuron (labeled with EGFP). Western blotting indicated that increased expression of ER chaperones, GRP78 and ORP150, reached a maximum by 7–12 days after infection (Fig, 2D, right portion). In contrast, there was no increase in these chaperones on the contralateral side (i.e. the side where the LoxPael-R adenoviral vector was replace by a LoxLacZ vector; Fig. 2D and E). Levels of a cytoplasmic chaperone, the 70 kDa heat shock protein, remained unchanged on both sides of the brain (Fig. 2D). These data indicate that co-infection of

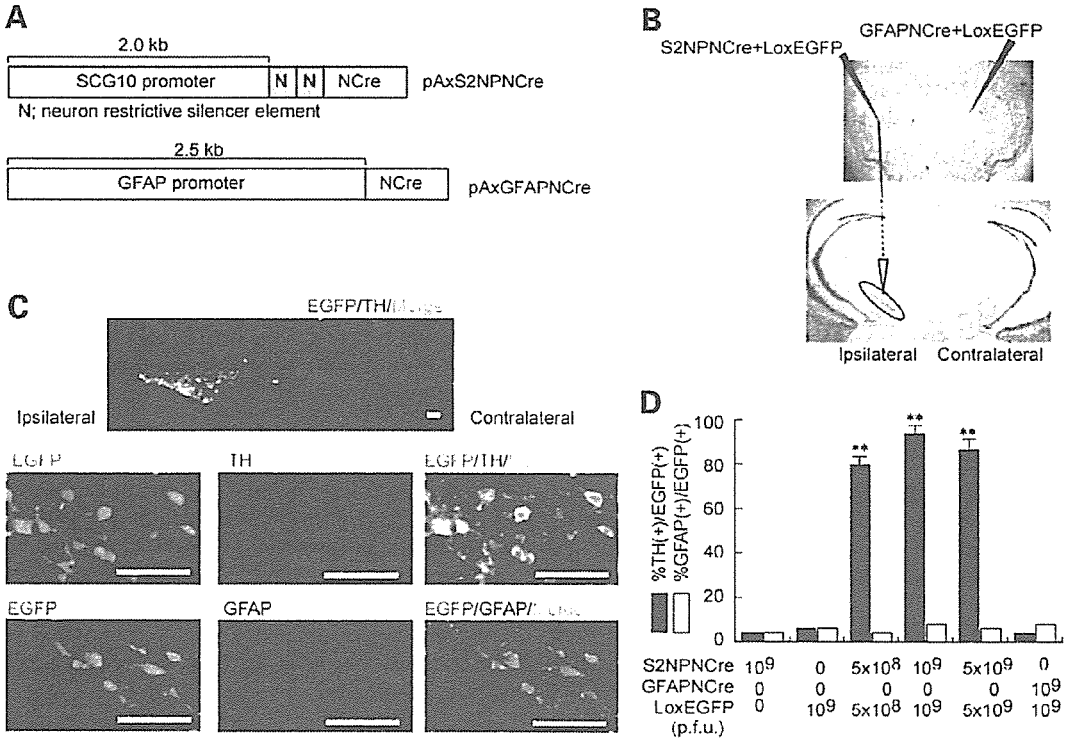

Figure 1. Neuron-specific expression of a transgene in the SNpc after adenoviral infection of the striatum. Two adenoviral vectors were constructed to drive cell type-specific expression of Cre recombinase in neurons (AxS2NPNCre also termed S2NPNCre) and astrocytes (AxGFAPNCre also termed GFAPNCre) (**A**). S2NPNCre was injected unilaterally along with LoxEGFP into the striatum (10^9 p.f.u., in each case) as shown (**B**, upper panel). 7 days after injection, brain slices corresponding to the striatum (B, upper panel) or SNpc (B, lower panel) were analyzed by Nissl staining. On the contralateral side, GFAPNCre was injected along with LoxEGFP (10^9 p.f.u., in each case). SNpc sections were analyzed by fluorescence microscopy using antibodies to TH or GFAP (**C**). Merged images are shown on the top and the far right (marker bar corresponds to 200 μm; note that magnification is greater in the lower panels compared with the top panel), and are representative of six repeat experiments, obtained at −3.1 mM from the Bregma. (**D**) Combinations of adenoviral vectors at the indicated concentrations were injected into the striatum of wild-type mice, and, 7 days later, animals were sacrificed and sections of SNpc were analyzed at five different levels (−3.16, −3.28, −3.40, −3.52 and −3.64 mM from the Bregma). Sections were subjected to image analysis in order to determine the area of TH-positivity [TH(+)] as a percentage of the area of EGFP-positivity [%TH(+)/EGFP(+)]. The mean ± SD is shown ($n = 6$), and ** denotes $P < 0.01$, compared to S2NPNCre infection alone.

LoxPael-R and S2NPNCre in the striatum caused expression of Pael-R in SNpc neurons, and triggered the ER stress.

Expression of Pael-R in SNpc of parkin$^{-/-}$ mice resulted in neuronal death

Parkin null mice (*Parkin*$^{-/-}$) were generated by replacing the proximal exon 3 with a neo cassette (PGK-neo) and two lox P sites (Supplementary Material, Fig. S1A). Southern blotting revealed homologous recombination of the mutant allele (Supplementary Material, Fig. S1B). Reverse transcriptase–polymerase chain reaction (RT–PCR) to detect Parkin transcripts confirmed the absence of normal transcripts in homozygous mutant mice (Supplementary Material, Fig. S1C). Sequencing of RT–PCR products confirmed complete deletion of exon 3 and a frame-shift downstream of exon 2 in mutant mice (Supplementary Material, Fig. S1D). Consistent with these data, western blotting with anti-Parkin antibodies showed the absence of Parkin antigen in brain samples (Supplementary Material, Fig. S1E). Parkin homozygous mutant mice were born at the expected mendelian ratio, showed no overt abnormalities (except a slight decrease in body weight) and had normal lifespans (18,19). Moreover, *Parkin*$^{-/-}$ mice were comparable, in terms of the number of TH-positive neurons in the SNpc, compared to wild-type littermates. However, *Parkin*$^{-/-}$ animals displayed a slight increase in striatal dopamine content, compared with wild-type littermates (not shown).

Parkin has been shown to ubiquinate Pael-R, thereby promoting degradation of insoluble and toxic Pael-R overexpressed in cell culture systems (6). Thus, we hypothesized that similar overexpression of Pael-R in *Parkin*$^{-/-}$ mice might result in severe ER stress and cell death in the SNpc. Using *Parkin*$^{+/+}$ and *Parkin*$^{-/-}$ mice, LoxPael-R was co-injected unilaterally into the striatum with LoxEGFP (as a neuronal marker) and S2NPNCre. Whereas up-regulation of Pael-R was confirmed by immunohistochemical analysis in the ipsilateral SNpc of both types of mice (white arrowheads in the lower panels of Fig. 3A indicate neurons positive with both TH and Pael-R), a marked decrease in the number of Nissl-positive neurons was demonstrated in *Parkin*$^{-/-}$ mice, (Fig. 3A and B). Neurodegeneration in the SNpc was accompanied by loss of TH immunointensity and decreased dopamine content in the striatum (Fig. 3C and D).

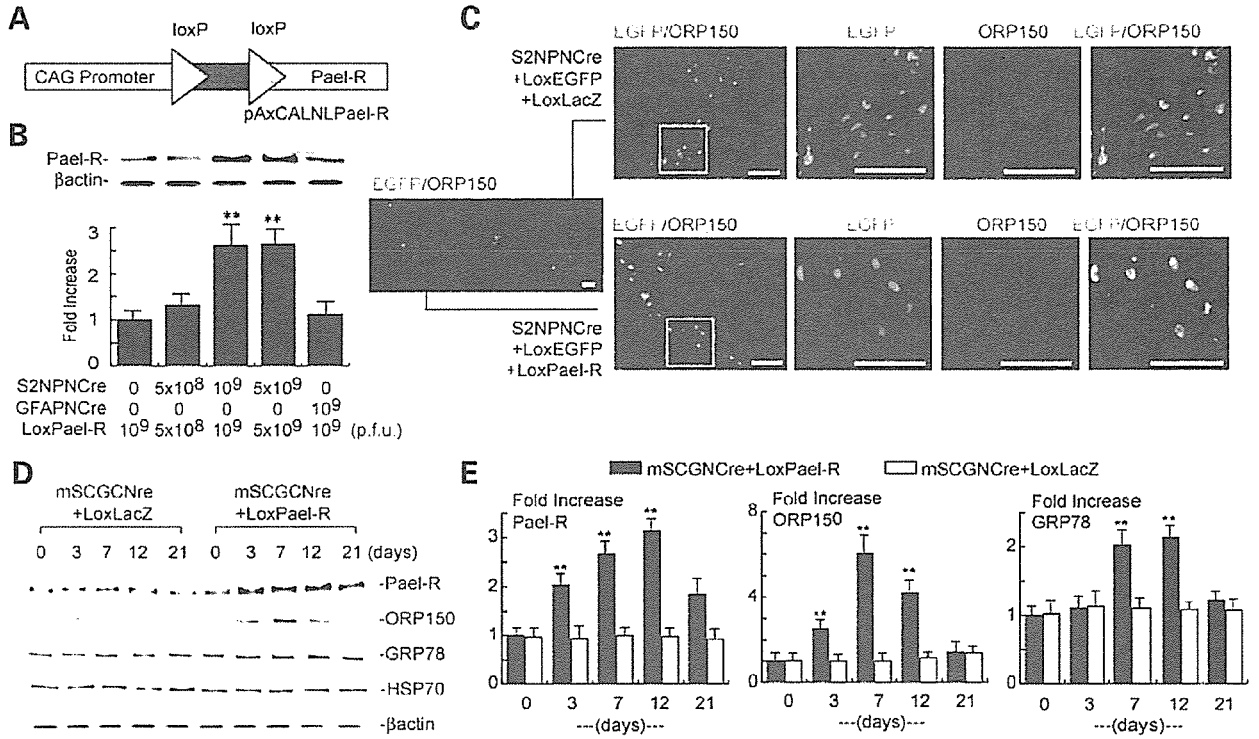

Figure 2. Transfection of Pael-R induces the ER stress in the SNpc. (**A**) Schematic depiction of the construct pAxCALNLPael-R to yield the adenoviral vector AxCALNLPael-R (LoxPael-R). A stuffer sequence (gray box) flanked by two lox-P sequences (arrowhead) was inserted between the promoter and *Pael-R* gene. (**B**) Adenoviral vectors carrying either S2NPNCre, GFAPCre or LoxPael-R were injected into the striatum as described in Figure 1, and, 7 days later, expression of Pael-R was assessed by Western blotting (upper panel), together with the levels of ß-actin as an internal control. Intensity of the corresponding bands was semi-quantitatively assessed by densitometric analysis and expressed in terms of fold-increase versus control samples where no adenovirus was injected (lower panel; $n = 6$, mean ± SD, and ** denotes $P < 0.05$ compared to LoxPael-R infection alone). (**C**) A mixture (total 2 μl) of adenoviral vectors including S2NPNCre (10^9 p.f.u.), LoxEGFP (5×10^8 p.f.u.), and AxCALNLNZ (LoxLacZ; 10^9 p.f.u.) was injected unilaterally in the striatum of C57Black/6J mice (upper panels). The same mixture was injected on the contralateral side, except that LoxLacZ was replaced by LoxPael-R (10^9 p.f.u.; lower panels). Seven days later, animals were perfusion-fixed and brainstem sections were immunostained using anti-ORP150 antibody (red). Merged images with EGFP signals (green) are shown in yellow. Open boxes indicated in the far left panels are magnified in the three panels on the right. Images are representative of six repeat experiments and the marker bar indicates 200 μm. (**D**) S2NPNCre + LoxLacZ (10^9 p.f.u., each) were injected unilaterally (termed ipsilateral) into the striatum, and S2NPNCre + LoxPael-R (10^9 p.f.u., each) were injected on the contralateral side. At the indicated time points, the brainstem was removed. The SNpc was separated and Western blotting was performed using antibodies to ORP150, GRP78, HSP70 and β-actin (images are representative of six repeat experiments). (**E**) Expression of Pael-R (left panel), ORP150 (middle panel), and GRP78 (right panel) on the ipsilateral (open bars) or contralateral side (closed bars) was assessed by densitometric analysis and is expressed as fold-increase versus control (day 0 indicates the day of the operation without injection of adenoviral vectors ($n = 6$, mean ± S.D is shown). ** denotes $P < 0.05$ by multiple comparison analysis compared to day 0 on the ipsilateral side.

No significant neuronal damage was observed in *Parkin*$^{+/+}$ mice after the overexpression of Pael-R using these methods.

To determine whether loss of TH staining in the SNpc, associated with increased expression of Pael-R, was due to neuronal death, we performed TUNEL analysis and monitored expression of a neo-epitope for activated caspase-3 (20). Increased expression of Pael-R in the SNpc, achieved as above (by unilateral injection of S2NPNCre, LoxPael-R and LoxEGFP; the contralateral side was injected with S2NPNCre, LoxLacZ and LoxEGFP as a control), demonstrated a small increase in DNA fragmentation even in the ipsilateral SNpc of wild-type mice (Fig. 4A and C). Increased DNA fragmentation was more striking in the ipsilateral SNpc of *Parkin*$^{-/-}$ mice, with maximal intensity 7 days after infection (Fig. 4B and C). The number of EGFP-and TUNEL-positive cells is significantly increased in the SNpc of *Parkin*$^{-/-}$ mice (Fig. 4B and C). It should be noted that there was a small increase in TUNEL staining on the contralateral side (Fig. 4C) observed most consistently in caudal sections (−3.4 and −3.6 from the Bregma). This might be due, at least in part, to crossed projections from the striatum to the contralateral SNpc. Pilot studies showed EGFP expression in the contralateral SNpc after unilateral injection of S2NPNCre and LoxEGFP, though this was <5% of the EGFP expression observed in the ipsilateral SNpc (not shown). Increased expression of Pael-R in the SNpc, achieved as above, demonstrated a small increase in the intensity of activated caspase-3 staining in the ipsilateral SNpc of wild-type mice (Fig. 4A and D). Expression of activated caspase-3 antigen was more striking in the ipsilateral SNpc of *Parkin*$^{-/-}$ mice (Fig. 4B and D), with maximal intensity 5 days after infection (not shown). The number of EGFP-positive cells costaining with activated caspase-3 is significantly increased in the SNpc of *Parkin*$^{-/-}$ mice (Fig. 4B and D).

Since there was no apparent damage, due to experimental manipulation or other factors, in the ipsilateral striatum (this